TU
WIEN

TECHNISCHE
UNIVERSITÄT
WIEN

DIPLOMARBEIT

Investigation of Novel Light Emitting Organic Materials Towards the Use as Optical Stimulator for Bio-Electronic Microdevices

Ausgeführt zur Erlangung des akademischen Grades eines
Diplom-Ingenieurs

Unter der Leitung von
O. Univ. Prof. Dr. Emmerich Bertagnolli
Ass.Prof. Dr. Heinz D. Wanzenböck
E362
Institut für Festkörperelektronik

Eingereicht an der Technischen Universität Wien
Fakultät für Elektrotechnik

von

Mathias Eberl
Mat.Nr. 0227302
Rosenbergen 58
2123 Unterolberndorf

Wien, 15. Mai 2016

....
Unterschrift des Studenten

Kurzfassung

Trotz der weiten Verbreitung von optischen Stimulatoren in der Medizintechnik sind einige Eigenschaften dieser Stimulatoren noch nicht optimal. Das liegt vor allem daran, dass für medizin-optische Untersuchungen Lichtemitter vorteilhaft sind, die nicht auf harten, sondern möglichst auf flexiblen Substraten in dünnen Schichten hergestellt sind, unter feuchten Bedingungen langfristig funktional bleiben und keine korrosiven Materialen freisetzen können. Darüber hinaus müssen diese Produkte wegen der hygienebedingten nur einmaligen Verwendbarkeit einfach und kostengünstig in der Herstellung sein.

Diesen Anforderungen werden die derzeitigen organischen Leuchtdioden (OLED: Organic Light Emitting Diode) nur unzureichend gerecht, weil die Herstellung der dünnen Schichten derzeit durch die Verwendung von Verdampfungsprozessen mit der damit zusammenhängenden Vakuumtechnik sehr aufwendig und damit teuer sind.

Daher soll in dieser Arbeit mit einer neuer Klasse von Licht emittierenden Benzolaminen gezeigt werden, dass es möglich ist, durch einfache Technologien unter Verwendung von so genannten Spin-Coating Prozessen einen medizintauglichen organischen optischen Stimulator herzustellen.

Die vorliegende Arbeit befasst sich daher mit der Untersuchung der im Institut für angewandte Synthesechemie der TU Wien hergestellten neuartigen Benzolamin-Molekülen auf ihre Verwendbarkeit als organischen Leuchtdioden. Diese Moleküle sollten die Einstellung der Emissionswellenlänge über einen weiten, medizinisch wichtigen Bereich der Fluoreszenzspektroskopie durch Anpassung der Moleküllänge erlauben. Darüber hinaus können diese Benzolamine wegen ihrer Löslichkeit in Spin-On-Verfahren verwendet werden und erfüllen damit die Anforderung nach technisch einfacher und damit preiswerter Herstellung.

Für die optische und die elektrochemische Charakterisierung der Benzolamine werden sowohl die pulverförmigen als auch die gelösten Ausgangsmaterialen mittels UV-Vis Spektroskopie und Photolumineszenz-Chromatographie untersucht. Diese Methoden geben Aufschluss über den Bandabstand des Materials sowie dessen charakteristische Wellenlänge, woraus wiederum die Farbe des ausgesendeten Lichts der Substanz bestimmt werden kann.

Bei der elektrochemischen Charakterisierung der Substanzen mittels Cyclovoltammetrie wird durch Vergleich der gemessenen Kurven mit dem bekannten Material Ferrocene als Referenz das HOMO-Energieniveau (Highest Occupied Molecular Orbit) der Substanzen bestimmt. Zusammen mit dem Bandabstand kann daraus das LUMO (Lowest Unoccupied Molecular Orbit) berechnet werden. Die

energetische Lage dieser Orbits ist entscheidend für die Wahl des Elektrodenmaterials und damit für die Injektion von Ladungsträgern in die aktive Zone der OLED.

Durch elektrooptische Messungen zeigt sich, dass sich die untersuchten Moleküle gut als Stimulatoren vom grünen bis zum blauen Spektralbereich eignen. Außerdem kann gezeigt werden, dass diese Materialien für die Verwendung des technisch einfachen Spin-Coating Prozesses für die Herstellung der Dioden gut geeignet sind.

Zur Demonstration der Funktion als optischer Stimulator wird abschließend aus den organischen Materialen eine organische Leuchtdiode erzeugt und der emittierte optische Photostrom vermessen sowie die Effizienz bestimmt.

Damit wird der Weg für biokompatible, flexible und robuste organische Lichtquellen und Lichtquellarrays für die lokale und ortsaufgelöste Fluoreszenzspektroskopie von Biomarkern geebnet.

Executive Summary

Despite the wide usage of optical stimulators in medical environments some of the properties of these simulators are not optimal. This is because for medical-optical examinations light emitters are beneficial which stay functional under humid conditions and do not release corrosive materials during operation. Moreover, these products have to be simple and cost efficient in fabrication because of the one-time-use with respect to hygienic reasons.

These requirements are currently fulfilled insufficiently by organic light emitting diodes (OLED) because the fabrication of the thin layers are currently only possible with the help of evaporation processes which is very sophisticated and expensive because of the necessary vacuum technology.

Therefore, this work should show with a new class of light emitting benzylamines the possibility to fabricate an organic optical stimulator which is suitable for biomedical applications with the use of simple fabrication technologies utilizing the Spin-Coating process.

This work deals with the investigation of novel benzylamine molecules which are assembled by the Institute of Applied Synthetic Chemistry of the TU Vienna for their applicability as organic light emitting diodes. These molecules should enable the possibility to adjust the emission wavelength over a wide, medically important range only through the adaption of the length of the molecules.

Moreover, because of the solubility of the benzylamines the molecules can be processed with a Spin-On-Process which fulfils the requirement for a technical simple and thereby cost efficient fabrication.

For the optical and electrochemical characterization of the benzylamines both the powdery and the dissolved base materials are analysed by UV-Vis spectroscopy and photoluminescence chromatography. The results of these methods offer the information about the band gap of the materials as well as about their characteristic wavelength what from the color of the emitted light can be determined.

For the electrochemical characterization of the substances with the help of cylcovoltammetry the measured graph is compared to the known reference material Ferrocene to determine the Highest Occupied Molecular Orbit (HOMO) of the molecule. Combined with results for the band gap of the materials the Lowest Unoccupied Molecular Orbit (LUMO) can be calculated. The energetic Position of these orbits is crucial for the choice of the electrode materials and therefore for the injection of charge carriers into the active zone of the OLED device.

With electro optical measurements it can be shown that the investigated molecules fit well as stimulators for the spectral range of green to blue light. Moreover, it can be shown that these materials can be utilized for the use of the technically simple Spin-Coating process for the fabrication of the Stimulators.

To demonstrate the functionality as optical stimulator an organic light emitting diode is fabricated with the investigated organic substances and the emitted optical photo current is measured as well as the efficiency of the device.

For this reason, the path for biocompatible, flexible and robust organic light sources as well as light source arrays for the local and space-resolved fluorescence spectroscopy of biomarkers is paved.

Contents

1 Introduction

Because of the increasing affords to monitor multiple bio-signals during the day as well as during medical attention the need for small, cheap and wearable biosensor increases. For such applications the sensing element as well as the displaying element have to be bonded together into one device which is easy to wear and displays immediately the status of the monitored bio-signal.

Because of the wearability such a device should be flexible to easily adapt to the form of the measured body. For this work the emitter in respect of two different sensor applications is investigated. One possible application would be a wearable blood-oxygen sensor which can be worn like a patch where both the light source and detector of light have to be flexible.[1]

Another application would be the possibility to stimulate nerve cells with blueish light from an OLED to activate specific areas of nerve tissue to investigate the network functionality of neurons or to trigger fluorescence markers in Caco2 cells to continuously monitor the grow of the cells. Recent investigations suggested that OLEDs are an ideal platform technology for investigating and controlling biological processes with single cell resolution. [2]
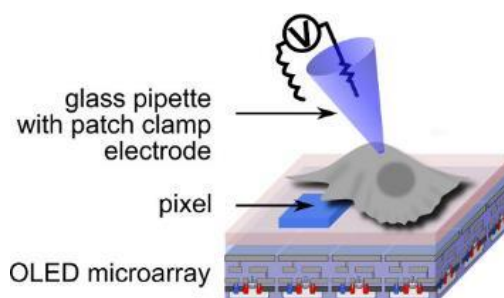
Figure 1.1: Application of OLED microarray as stimulator for neural cells.[2]

This work should investigate the fabrication of an OLED for a lab-on-a-chip microdevice to monitor the grow and interaction of living cells like Caco2 cells or neurons as shown in Figure 1.2. Because of the beneficial properties the light source for the stimulation of the cells should be fabricated with novel organic light emitting materials which should be beneficial for the stimulation. Therefore, a setup is contemplated where the OLED emits blue light from below the cell sample through the glass substrate. Depending on the investigated cell culture the blue light stimulates either fluorescence marker or directly stimulates the cells e.g. neurons. The fluorescence light will be detected by the photodetector array which is mounted on top of the setup and is filtered by a polarizer.
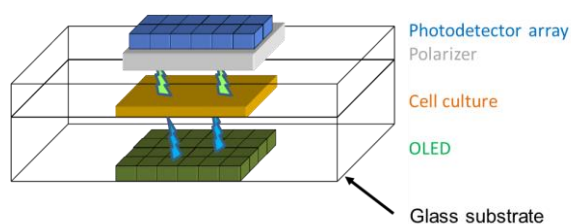
Figure 1.2: Schematics of the setup of an OLED microarray as stimulator for cell cultures.

The current progress in the general OLED technology is very high but the first discovery of the electroluminescence in organic semiconductors, which was in the year 1963, excited little interest at that time.[3] Around 20 years later Tang and VanSlyke managed to significantly improve the properties of the OLED devices to gain efficient, low voltage electroluminescence in an organic thin film device.[4]

For display applications in portable devices the most important factor is the power consumption which has to be minimized to rise the battery lifetime. There the emissive organic display has the advantage that light contributing power is spent only when a pixel is turned on. Besides that, the required voltage levels to drive the pixels are smaller for OLEDs which make them safer to use them in medical applications.

As mentioned before OLEDs are very fast devices with response times in the microsecond range which is much faster than any commercial LCD technology. Besides that, the thin film nature of the organic LED features almost no lateral conduction which enables the possibility to produce pixel in the micrometer range. Moreover, the light emission is quasi-lambertian, resulting in a wide viewing angle.

A big concern of the present research is to increase the efficiency and lifetime of the OLED devices. Normally organic materials are very susceptible to moisture and oxidation which degrade the organic material and significantly decrease the lifetime of the devices. Therefore, special housings and passivation layers are used to enclose the device which also protects organic cells from interaction which the OLED. To increase the efficiency of the device new materials as well as different multilayer designs are investigated.[5]

This work covers several topics of the fabrication and investigation of organic materials and their use for light emitting diodes:

- Electro-chemical and photo-optical characterization of several new organic substances for their general characterization

- Determination of the optimum process parameters to fabricate a simple OLED by spin-coating the organic materials

- Deposition of the cathode material with the help of a shadow mask for structuring

- Construction of an evaporation setup and deposition of electron- and hole-transport-layers as well as the organic emitting layer by thermal vacuum deposition

- Electrical and electro-optical characterization of the OLED Devices

The characteristics of the organic materials should give information about a possible applicability of the materials for light emission by electrical stimulation. Furthermore, the characteristic values of the organic are also important for the color of the emitted light and the selection of attached electrodes.

The fabrication and characterization of simple OLED devices with the organic materials should prove that these materials can be used as organic light emitting layer in different applications.

2 Theory

This chapter is an overview of the function of organic molecules as conductive light emitting materials and the technical realization to use them for light emitting diodes. Therefore, the following pages give an insight into the luminescence mechanisms and the general layout of an OLED device.

## 2.1 Organic Light Emitting Diodes (OLEDs)

Organic light emitting Diodes do have nearly similar behavior like normal diodes but instead of a semiconductor material with two different dopings only one organic layer is used. Therefore, the simplest version of an OLED is a specific organic material in between two metal electrodes which can emit light if a characteristic voltage is applied to the electrodes. This characteristic voltage can vary depending on many factors like the electro-chemical properties of the material, the thickness of the layer, the size of the pixel, the electrode material and so on. This can cause strong variations of the quantum efficiency. Because the area between the electrodes behaves like a point source of light it is advantageous to couple out the light through an electrode which is normally done with the help of a transparent indium tin oxide (ITO) anode. [6] [7] [8] [9]

To get a better understanding of OLEDs the conduction mechanisms, the general function and a possible approach for the technical realization of OLEDs are discussed in the following subchapters.

2.1.1 Conduction Mechanisms of Organic Materials

Organic Semiconductors consist of Van-der-Waals bound molecular units instead of covalent bound units as in non-organic solids. Therefore, they feature a small conductivity and a big band gap. The organic molecules normally consist of hydrocarbons with conjugated double bonds.[10]

An example of such a hydrocarbon compound is benzol. In such a molecule the molecular orbits (MO) can be determined by investigating the occupation of the 2s- and 2p-orbits of the carbon which are responsible for the linking. In the normal configuration the carbon has one 2s-orbit and three 2p-orbits (Figure 2.1a). By an overlapping of the orbits hybrid orbits are formed which can for example happen if two 2p-orbits are combined with the 2s-orbit of the carbon. This results in three equivalent sp^2-orbits which are in the same plane but 120° shifted to each other (Figure 2.1b).
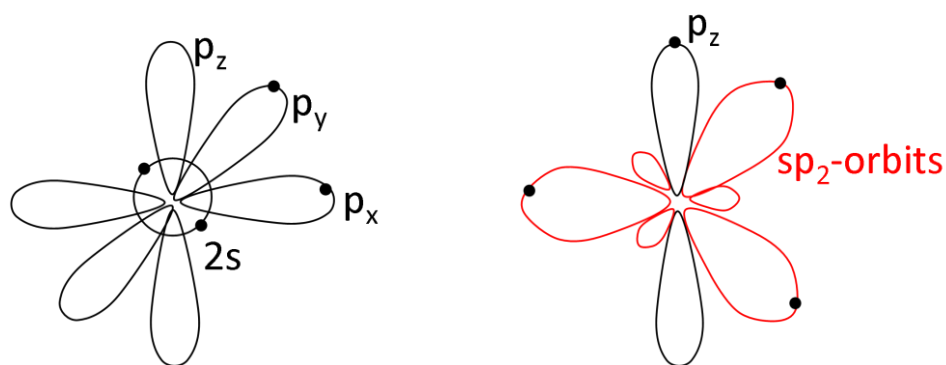
Figure 2.1: Schematics of normal orbits of carbon (a) and sp₂ hybridization of carbon (b)

For the connection of this structure to another carbon atom one so called σ-bond is established and one π-bond can be established between the p_z-orbits.[a]

In this configuration the π-electrons of a benzol-ring are not distributed cylindrically like at the σ-bond. Therefore, the electrons of the π-bond are delocalized over the whole molecule which allows an efficient carrier transport in the molecule. This special case is indicated by the chemical structure formula of the benzol (Figure 2.2) which shows an electron-ring in the middle instead of defined bindings.
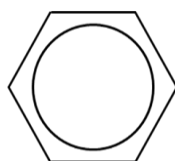
Figure 2.2: Schematic of Chemical structure of benzol

In this case the lowest bond π-orbits are filled with π-electrons and all higher non-binding orbits stay unoccupied. The energetic Highest Occupied Molecular Orbit (HOMO) and the Lowest Unoccupied Molecular Orbit (LUMO) are important for the electrical and physical characteristics of the molecule. The HOMO and LUMO are separated by an energy gap which is crucial for the electrical characteristics

---

[a] A σ-bond bond is the strongest type of covalent chemical bond but only possible as a single bond between atoms. If there is more than one bond between atoms (e.g. double bond, triple bond) it consists of one σ-bond and the other bonds are π-bonds. A π-bond arises if two elements are small in size and therefore can form short bonds. Due to these short bonds, when two atoms like carbon and oxygen form a sigma bond, they are so close together that an energy level (orbital) of carbon overlaps with an energy level (orbital) of oxygen. This forms a π-bonds where electrons orbit around.

and the wavelength of the light which can be emitted when electrons recombine. Only some molecules with such a suitable chemical structure are able to emit light at electrical stimulation as for example in organic light emitting diodes.

## 2.1.2 Functionality of Organic Light Emitting Diodes (OLEDs)

A simple OLED generally consist of a transparent anode (commonly ITO is used), an organic emitting layer of a selected molecule and a metal cathode as illustrated in Figure 2.3.

Figure 2.3: Architecture of a Single Layer OLED.

To induce charge carriers to activate the device a positive voltage has to be applied to the ITO anode. Depending on the cathode material, organic material and the thickness of the organic layer the device gets conductive at an ascertained voltage. As mentioned before charges are injected to the organic layer, electrons at the cathode and holes at the side of the anode. Depending on the thickness of the organic layer, the carrier mobility and the injection properties the charges can recombine in the organic layer by the emission of light. In a worse case the organic layer can be very thin and the injection of one charge carrier (e.g. holes) is much better than of the other which can result in the recombination of the charges at the opposite electrode (e.g. cathode) without the emission of light.[11]

More sophisticated devices consist of many layers with different functions such as a Hole- or Electron-Injection-Layer or a Hole- or Electron-Transport-Layer (HTL/ETL). These layers can increase the efficiency of the device by transport the charge carriers more effectively from the electrodes to the emitting material where they recombine and emit light. Such layers also avoid that the recombination of the carriers happens on the electrodes which also increases the efficiency of the light output.
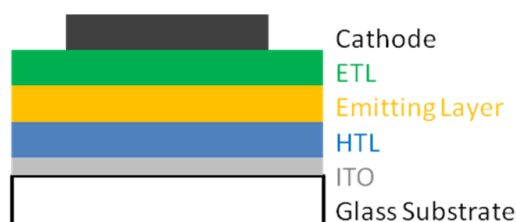

Figure 2.4: Architecture of a Multi-Layer OLED.

The additional layers improve the fitting of the work function of the metal electrode the HOMO and LUMO level of the organic material to achieve a higher conductibility for improved carrier transport.

The work function of a material is defined by the energy which is needed to move an electron from a solid to a point immediately outside the solid surface or in case of semiconductors the energy which is needed to move an electron from the Fermi level into vacuum.

As mentioned before a transparent and conductive anode material has to be used to get a back emitting device. Such a material is Indium Tin Oxide (ITO) which has a work function of 4.8eV (4.5-5.1eV)[12] is commonly used. This material layer is normally deposited on a glass substrate whereby the refractive index of the glass and the ITO does not fit perfectly which causes a slightly loss of emitted light due to backscattered light. On the other side the amount of materials which are applicable for the cathode is more versatile whereas a low work function metal (Mg, Ca, Li, Al) or a metal alloy (MgAg) is required to improve the injection of electrons into the organic material layer. The small work function material results in a small effective injection barrier height at the metal electrode/ organic layer interface.[13] Such metals have the drawback of a relatively high reactivity in air so they do not fit for most operation environments. A passivation layer has to be added to encase the metal and the organic material. Otherwise the properties of the device degrade very fast.
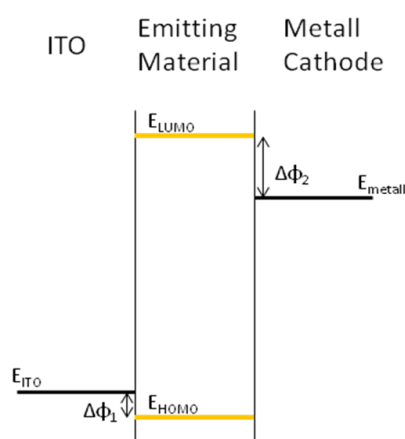
Figure 2.5: Schematic of the energy levels of a single layer OLED.

In Figure 2.5 the energy levels of a single layer device are shown where the energetic barriers are different and therefore the hole and electron injection into the emitting material is different. Besides that the mobility of the carriers can also differ in the organic material which results in lower quantum efficiency. If the organic layer is too thin or the mobility of the carriers is too high then the carriers diffuse through the emitting layer and recombine on the counter electrode which results in no radiation of light. Therefore, ETL (e.g. Alq3) and HTL (e.g. PEDOT:PSS) are often used in multi-layer devices to improve the emissive properties and to increase the output of photons.

Furthermore, a thin layer of lithium-fluoride (LiF) between the organic layer (respectively the electron transport layer if it exists) and the cathode improves the injection of electrons and enhances the

performance of the device[14]. The thickness of such a LiF layer is very important for the efficiency of the device because a thin layer less than 1nm and a very thick layer above 15nm decrease the electroluminescent performance whereas a layer of about 3nm results in a good characteristic. Besides the good electron injection properties of the LiF, the material normally is a superior insulating material which features the highest band gap energy of 12eV among oxides and fluorides.

An accurate fabrication as well as the combination of a suitable material mix of the electrodes and organic layer is crucial for a proper operation of such an OLED device.

2.1.3 Technical Realization

In most cases the layout of an organic light emitting diode is build up as a multi-layer device like in Figure 2.6 where the diode emits through the transparent substrate. However, for some applications it would be useful if the emission is in the other direction which can be achieved with a transparent cathode. Such a device is called a Top-emitting OLED (TOLED) and is commonly used for active matrix displays. The drawback of these top-emitting was the more difficult device fabrication as well as the lower efficiency and lifetime. These disadvantageous properties have been studied and improved by many researchers over the last years and show now nearly similar behavior like bottom-emitting OLEDs.
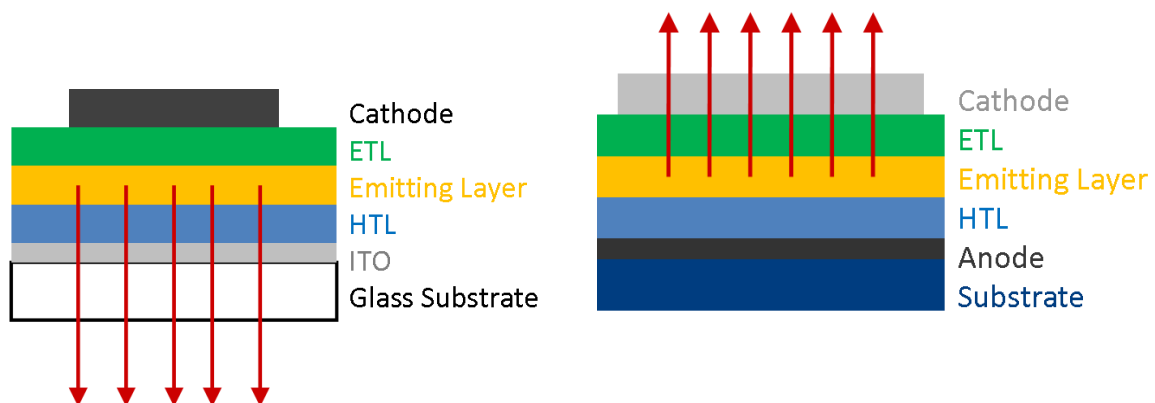
Figure 2.6: Button transmitting OLED with emission of light through the glass substrate

Figure 2.7: Top-emitting OLED (TOLED) with emission of light through the top cathode

Another layout of OLEDs is the transparent OLEDs which were first demonstrated in 2002.[15] These devices are inverted top emitter with ITO as cathode and semitransparent gold as anode. Voltage and efficiency are comparable to normal substrate emitting devices.

2.2 Characterization Methods

For a suitable device design the characterization of the organic material is essential to determine the molecular energy levels, the band gap as well as the electrical and optical properties. The determination of the energy levels by cyclic voltammetry is important for the choice of the electrode materials and for the use of charge transport layers. The band gap can be referred to the wavelength of the emitted light and is for this reason a key property of the material. For the determination of the conductivity and quantum efficiency the electrical and optical characteristics are measured.

2.2.1 Cyclic Voltammetry (CV)

The cyclic voltammetry is part of the electro-analytical chemistry and is used for the investigation of the oxidation and reduction processes in non-organic and organic chemistry. For this work the measurement technique is used for the determination of the HOMO- und LUMO-levels of the organic substances. These levels are related to the conduction and valence band and therefore important values of an organic LED.

If the work function of the electrode material is known it can be estimated if the substances are suitable for hole or electron conduction. The energy barrier between the material of the electrode and the organic material should be as small as possible.[16]

At a cyclic voltammetry experiment electrodes are dipped into an electrolyte solution and depending on the applied voltage the phases of electron and ionic conductors are interacting. The electrodes used for these measurements are classified as polarizing and non-polarizing electrodes. Non-polarizing electrodes (e.g. Ag/AgCl electrodes) do not change their potential at different currents which make this type suitable as reference electrode. Polarizing electrodes are used as working electrodes because of no charge transfer between the metal surface and the electrolyte at an ascertained potential range.

If a positive or negative potential is applied to the working electrode an electro-chemical double layer is built up that consists of molecules and ions which are specifically absorbed to the electrode surface (inner Helmholtz-Layer). In a certain distance another layer of ions of the opposing charge is built up (outer Helmholtz-Layer). Adjacent a diffuse layer accumulate to the electrode whereas the density of charges decreases with the distance to the electrode. The thickness of the diffuse layer is proportional to the applied potential.

If the potential difference between the electrodes reaches a certain value a current starts to flow. The relevant Faraday current starts if the decomposition voltage is reached. Thereby the Faraday current has to be much higher than the capacitive current to differentiate these two currents. Reduction arises if the energy level of the electrode is lowered so electrons are transported from the electrode to the

LUMO of the electrolyte. Oxidation occurs if the potential of the working electrode is raised until electrons of the HOMO of the electrolyte are dispensed. These two events can be seen in the CV-diagram by a rise of the current density if the applied potential gets closer to an energy level of a molecular orbit and a fall of the current density if the energy level is passed.[17]

Reduction
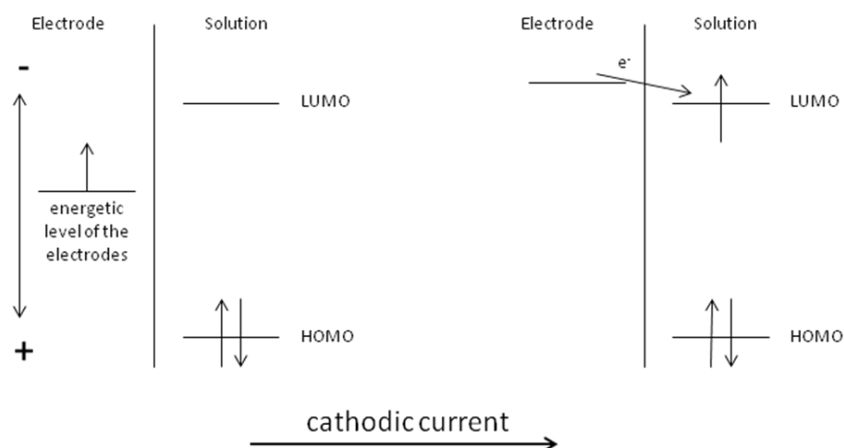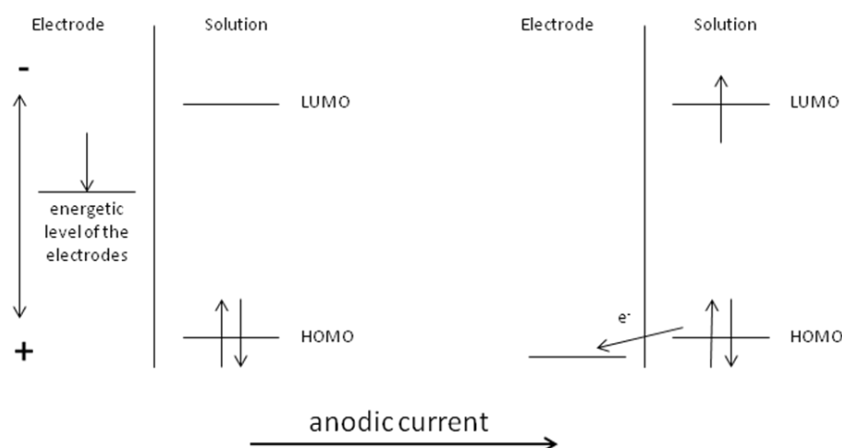

Figure 2.8: Schematic of the reduction process.

If the potential E, which is applied to the electrode, is raised over the half-wave potential $E_{1/2}$ of the educt the ratio of the educt to product decreases according to the Nernst equation. Assuming similar activity coefficients of the oxidized C_{ox} and reduced C_{red} form the following Nernst law is valid:

$$\left(\frac{C_{ox}}{C_{red}}\right)_{x=0} = \exp\left(\frac{nF}{RT}\left(E - E_{1/2}\right)\right)$$

(2-1)

As described above reduction occurs if the negativity of the electrode is higher than the LUMO of the solution. In this case electrons from the electrode are transferred to the solution.

Oxidation

Oxidation occurs if the potential of the electrode is more positive than the HOMO level. At this case the electrons of the HOMO are able to be transferred to the electrode.

Figure 2.9: Schematic of the oxidation process.

In a common cyclic voltammetry experiment there are three electrodes used, a working electrode, a counter electrode and a reference electrode. As working and counter electrode usually solid electrodes like platinum or gold are used as well as electrodes with a drop of mercury. The reference electrode can be a silver/silver-chloride (Ag/AgCl) or a saturated Calomel electrode (SCE). The measured current flows between the working and counter electrode to make sure the reference electrode is not harmed at higher measurement currents. The reference electrode is only used as voltage reference at the measurement.

For a usual measurement four important parameters have to be set:

1. start potential

2. upper and lower return potential

3. scan speed

4. number of cycles

The start potential is applied at the beginning measurement to the working electrode. Afterwards the potential is raised during the measurement until the upper return potential. After reaching the upper return potential the applied potential is decreased until the lower return potential where the alteration is reversed again until the potential returns to the start potential. The scan speed $v = dE/dt$ is one of the most important factors of the measurement because of the build-up of the layers. Differences in

the scan speed results in a different thickness of the Helmholtz layers and therefore in different current densities. The scan speed can nowadays be up to 10kV/s whereas 50mV/s is a common value. To make sure that the solution stays conductible during the experiment a conductive salt is mixed into the solvent with a concentration of about 0.1mol/l. At a cyclic voltammetry experiment no absolute potential can be measured. Hence, the potentials are referred to a reference electrode such as a silver/silver-chloride (Ag/AgCl) or a saturated Calomel electrode (SCE). Another approach is to refer the potential to a well known reduction (redox) potential of a material such as Ferrocene. To get the desired energy levels Ferrocene is measured in the given experimental setup and the obtained potential values can be referred to the energy values of this substance.
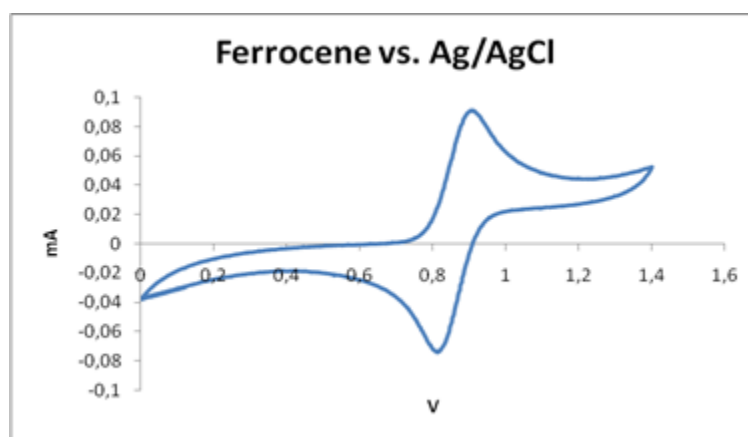
Figure 2.10: Cylic Voltammetry measurement of Ferrocene (0.5mM dm^{-3}) in tetra-n-butylammonium perborate (0.1M dm^{-3}).

To determine the absolute potential of the HOMO of a molecule the lowest half wave potential has to be measured. Afterwards this value is referred to a known substance such as Ferrocene which has a HOMO energy level of -4.8eV versus vacuum.[18] The difference of the oxidation potentials of the molecule which has to be characterized and Ferrocene can be directly referred to the energy levels of the molecular orbits.

The obtained values of the HOMO and LUMO levels can be used to find suitable electrode materials for a working OLED device. The difference between these two levels can also be referred to the band gap which defines the wavelength and therefore the color of the emitted light. The band gap of a substance can also be obtained by measuring the wavelength of the emitted light with photoluminescence measurements as described in the following chapter.

2.2.2 Optical Spectroscopy

Optical spectroscopy is a contactless measurement where the material under test is irradiated by light of a certain wavelength and either the absorption of the light or the emission of light of a different wavelength can be measured.

2.2.2.1 Ultraviolet–Visible Spectroscopy

Ultraviolet and visible (UV-Vis) absorption spectroscopy is the measurement of the attenuation of a beam of light after it passes through a sample or after reflection from a sample surface. Absorption measurements can be at a single wavelength or over an extended spectral range. Ultraviolet and visible light are energetic enough to promote outer electrons to higher energy levels, and UV-Vis spectroscopy is usually applied to molecules or inorganic complexes.

Many molecules absorb ultraviolet or visible light. The absorbance of a material increases as attenuation of the beam increases. Absorbance is directly proportional to the path length b and the concentration c of the absorbing species. Beer's Law states that the absorbance $A = e*b*c$, where e is a constant of proportionality, called the absorptivity.

Different molecules absorb radiation of different wavelengths. An absorption spectrum will show a number of absorption bands corresponding to structural groups within the molecule. For example, the absorption that is observed in the UV region for the carbonyl group in acetone is of the same wavelength as the absorption from the carbonyl group in diethyl ketone.

The absorption of UV or visible radiation corresponds to the excitation of outer electrons. There are three types of electronic transition which have to be considered:

1. Transitions involving p, s, and n electrons

2. Transitions involving charge-transfer electrons

3. Transitions involving d and f electrons

When an atom or molecule absorbs energy, electrons can rise from their ground state to an excited state. In a molecule, the atoms can rotate and vibrate with respect to each other. These vibrations and rotations also have discrete energy levels, which can be considered as being packed on top of each electronic level.
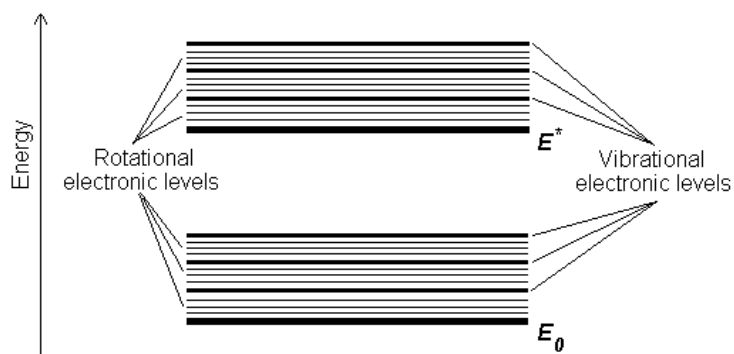
Figure 2.11: Schematic of the energy levels of absorbing species containing p, s, and n electrons

Absorption of ultraviolet and visible radiation in organic molecules is restricted to certain functional groups (chromophores) that contain valence electrons of low excitation energy. The spectrum of a molecule containing these chromophores is complex. This is because the superposition of rotational and vibrational transitions on the electronic transitions gives a combination of overlapping lines. This appears as a continuous absorption band.

Possible electronic transitions of p, s, and n electrons are:

- s - s* Transitions

  An electron in a bonding s orbital is excited to the corresponding antibonding orbital. The energy required is large.

- n - s* Transitions

  Saturated compounds containing atoms with lone pairs (non-bonding electrons) are capable of n → s* transitions. These transitions usually need less energy than s → s * transitions.

- n - p* and p - p* Transitions

  Most absorption spectroscopy of organic compounds is based on transitions of n or p electrons to the p* excited state. This is because the absorption peaks for these transitions fall in an experimentally convenient region of the spectrum (200 - 700 nm). These transitions need an unsaturated group in the molecule to provide the p electrons.

The UV-Vis spectral range is approximately 190 to 900 nm, as defined by the working range of typical commercial UV-Vis spectrophotometers. Purging a spectrometer with nitrogen gas extends the short wavelength limit to 175 nm. Working beyond 175 nm requires a vacuum spectrometer and a suitable UV light source. The long-wavelength limit is usually determined by the wavelength response of the detector in the spectrometer. High-end commercial UV-Vis spectrophotometers extend the measurable spectral range into the NIR region as far as 3300 nm. The light source is usually a deuterium

discharge lamp for UV measurements and a tungsten-halogen lamp for visible and NIR measurements. The instruments automatically swap lamps when scanning between the UV and visible regions. The wavelengths of these continuous light sources are typically dispersed by a holographic grating in a single or double monochromator or spectrograph. The spectral bandpass is then determined by the slit width of the monochromator or by the array-element width in array-detector spectrometers. The detector in single-detector instruments is either a photodiode, a phototube or a photomultiplier tube (PMT)
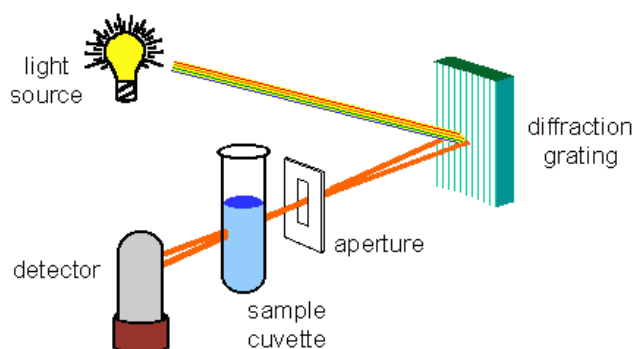
Figure 2.12: Schematic of a wavelength-selectable, single-beam UV-Vis spectrophotometer.[19]

Most commercial UV-Vis absorption spectrometers use one of three overall optical designs: a fixed or scanning spectrometer with a single light beam and sample holder, a scanning spectrometer with dual light beams and dual sample holders for simultaneous measurement of P and Po, or a non-scanning spectrometer with an array detector for simultaneous measurement of multiple wavelengths.[19]

2.2.3 Photoluminescence

Photoluminescence (PL) is the spontaneous emission of light from a material under optical excitation. The excitation energy and intensity can be chosen to probe different excitation types and also different parts of the sample. PL investigations can be used to characterize a variety of materials parameters. Features of the emission spectrum can for example be used to identify impurity levels. Under pulsed excitation, PL intensity transients yield lifetimes of excited states. In addition, thermally activated processes of non-radiative recombination cause changes of PL and can be investigated by this way.

Photoluminescence

PL analysis is a contactless and nondestructive form of measurement. Usually a low wavelength laser is used for optical pumping of electrons of the sample material into higher states. Afterwards the emitted light of the sample is filtered with a spectrometer and the photons are counted with a photomultiplier-tube (PMT).
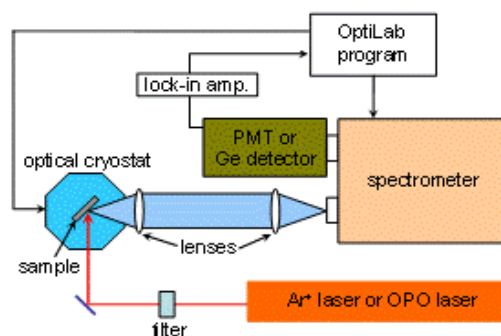
Figure 2.13: Typical experimental set-up for PL measurements.

The technique requires very little sample manipulation or environmental control. When light of sufficient energy is illuminating a material, photons are absorbed and (electron) excitations are created. These excitations relax and emit a photon. The PL can be collected and analyzed to provide information about the photo-excited states. The measured spectrum reveals transition energies and the PL intensity gives an estimation of the relative rates of radiative and non-radiative recombinations. Variation of the PL intensity upon change of external parameters, e.g., temperature, excitation energy, power of excitation, can be used to further characterize electron states and bands.

Photoluminescence excitation spectroscopy

In PL spectroscopy, which is performed at a fixed excitation energy, the luminescence properties are generally investigated, while photoluminescence excitation spectroscopy (PLE), which is carried out at a fixed detection energy, provides mainly information about the absorption properties and probes excited states of optical centers. At PLE the sample is excited by photons of the energy (ℏn) tuned to be absorbed by specific optical centers. Therefore, this technique requires a tunable excitation source. The high resolution PLE, i.e., the combination of highly resolved PL spectra as a function of the well-defined excitation energy provides detailed information about the system under investigation.

Applications for Photoluminescence Spectroscopy

Band gap determination: The most common radiative transition in semiconductors is between states in the conduction bands and in the valence bands where this gap is the bandgap of a semiconductor. Bandgap determination is particularly useful when working with new compound semiconductors.

Impurity levels and defect detection: Radiative transitions in semiconductors also involve localized defect levels. The PL energy associated with these levels can be used to identify specific defects, and the PL intensity can be used to determine their concentration.

Recombination mechanisms: As discussed above, the return to equilibrium, also known as "recombination" can involve both radiative and nonradiative processes. The PL intensity and its dependence on the level of photo-excitation and temperature are directly related to the dominant recombination process. Analysis of PL helps to understand the underlying physics of the recombination mechanism.

Material quality: In general, nonradiative processes are associated with localized defect levels, whose presence is detrimental to material quality and subsequent device performance. Thus, material quality can be measured by quantifying the amount of radiative recombination.[20]

2.3 OLED as Excitation Source for Biosensors

Substantial research efforts have been dedicated to the development of lab-on-a-chip (LoC) technologies, which offers a miniaturized platform for sample processing and can be used to perform numerous life science analyses.

While there have been numerous breakthroughs in the microfluidics of LoC bio-detection systems, much of the detection methodologies still rely on external lab-scale systems.[212223] However, there is a strong desire for completely portable LoC systems for point-of-care applications. Given its high degree of sensitivity, many research groups have tried to integrate fluorescence/photoluminescence (PL) detection techniques into LoC, where also organic light emitting diodes (OLEDs) are used as an excitation source and sometimes organic photodiodes (OPDs) as a means of detection.

Since OLEDs are comprised of thin films deposited by low temperature techniques, they can be easily integrated with most polymer/plastic microfluidic systems (for example, by depositing on the backside of a polydimethylsiloxane (PDMS) microfluidic channel). The capability to fabricate miniaturized OLED pixels is also ideal for LoC, where the microchannel size can be on the order of an individual pixel size.

Because the emission and absorption peaks of OLEDs are easily tuneable and only depending on the choice of the length of the molecule and their functional groups, these organic electronic devices are excellent candidates for more advanced detection systems.[24]

Different researches were performed concerning the test for alcohol and lactate in addition to glucose with alcohol oxidase (A_{Ox}) and lactate oxidase (L_{Ox}).[2526] A sample design of the fabricated LOC from this work is illustrated in Figure 2.14.
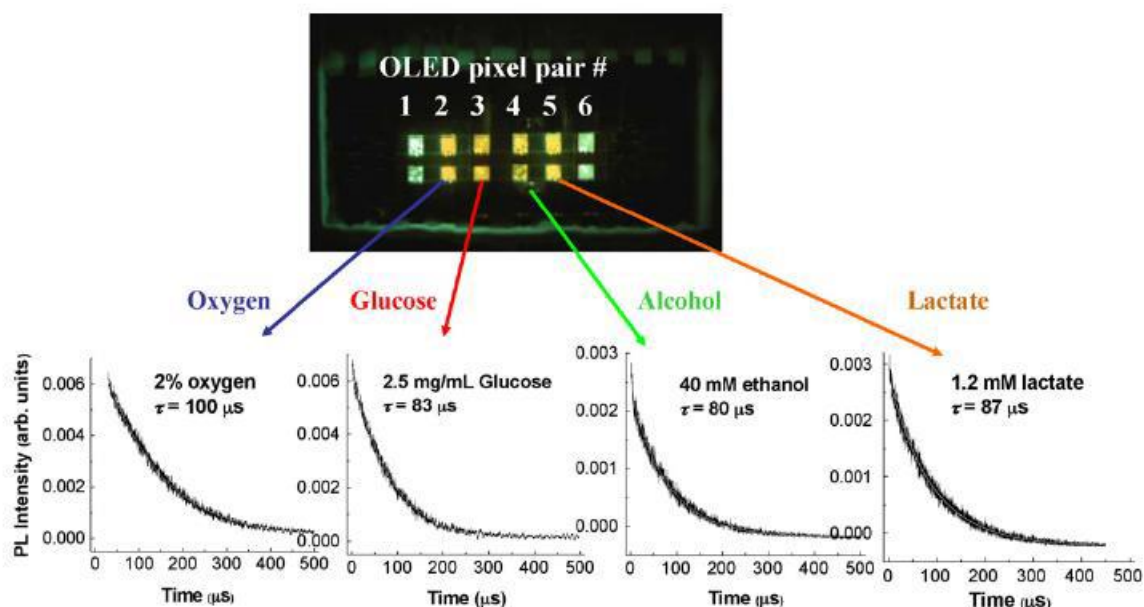
Figure 2.14: Structurally integrated OLED sensor for LoC sensing of oxygen, glucose, alcohol and lactate, with associated photoluminescence decay graphs.[27]

As a point of interest, the decay time of the different materials range from 30 ns up to about 100 μs. This difference in decay time can be used to improve the signal to noise ratio by offsetting the excitation and the detection.[24]

Another research group has discovered that the lighting used in smartphone displays can activate live cells that are genetically programmed to respond to light. OLEDs are used to "turn on" individual cells in the lab which is promising to control the cells optically to investigate the cell behaviour in cultured neuronal networks, brain slices, and other biomedical research applications.

As described in the paper Embryonic kidney cell line were tweaked to produce a light-sensitive protein which reacts to the exposure of blue OLED light from pixels directly underneath the cell as illustrated in Figure 2.15. Hence, the electric activity of individual targeted cells could be stimulated, while neighboring cells remained in the dark and stayed inactive.
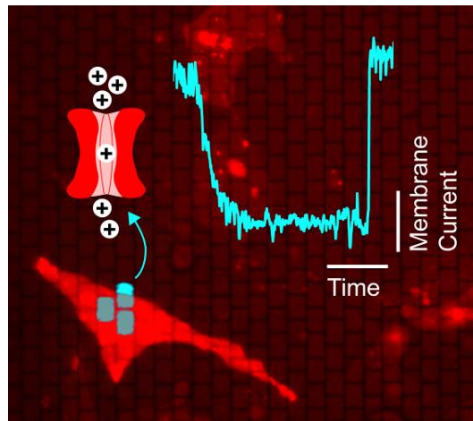
Figure 2.15: Use of a miniature version of an OLED displays to illuminate individual live cells with light-gated ion-channel embedded in their membrane, which facilitates optical switching of the membrane current with single-cell resolution.[2]

In literature a standard cell line is used to test the approach, but the goal is to activate individual neurons, which would facilitate a new way of studying neuronal network functions.[2]

Another research improved a fully integrated system by replacing a halide lamp excitation source with a green-emitting Alq3 OLED which is illustrated in Figure 2.16. With this setup an increase in the limit of detection was observed. With optimization of channel depth, responsivity of the photodiode and increase of the OLED output power, an improved detection limit should be feasible. Moreover, by reducing of noise artefacts within the associated system electronics (including connecting wires, lock-in amplifier, …), the detection limits are may also be decreased even further.[28]
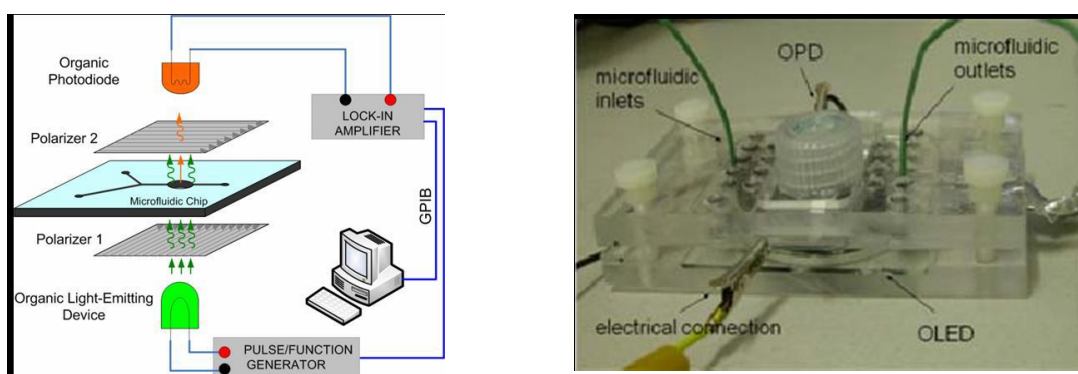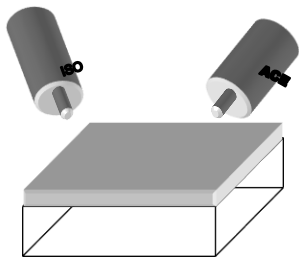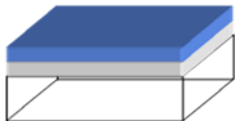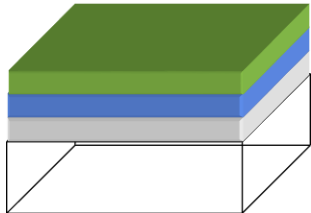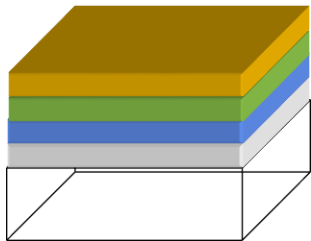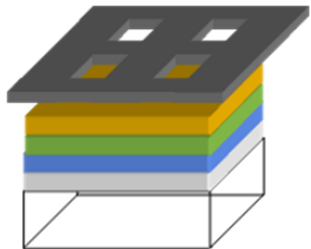
Figure 2.16: Illustration and photograph of a fully integrated organic light emitting diode-organic photodetector-lab-on-a-chip detection system.[28]

3 Experimental

3.1 Process overview

The following sequence gives an overview over the general device fabrication of a multi-layer organic diode. The crucial processing steps as well as the subsequent measurements are carried out in short time to avoid unwanted interaction with impurities or rather degradation of the processed substances at ambient air.

1)		Cleaning of an ITO-glass-slide with acetone and isopropanol in an ultrasonic bath.
2)		Spin-coating of the hole-injection-layer.
3)		Spin-coating of the organic emitting layer.
4)		Evaporation of an electron injection layer.
5)		Physical vapor deposition (PVD) of structured metal cathodes with the help of a shadow mask.
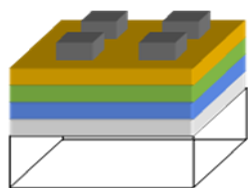
6)		Completed device.

Figure 3.1: Schematics of the process steps to produce an OLED.

3.2 Materials

For the fabrication of OLED devices a wide variety of materials can be used for the injection-, emitting-, transport- or metal-layer. This variety offers the opportunity to specifically adapt the transport and injection layers as well as the cathode material to the emitting layer to increase the performance of the diode. For a basic OLED design with novel emitting layers known substances are used in a first step to be able to compare the characteristics of the device with published values.

3.2.1 Electro-organic Materials

As organic material for the emitting layer of the device a wide variety of different substances are tested. All of the substances were synthesized by the Department of Inorganic-Chemistry of the Vienna University of Technology. The following table shows the name, structure, chemical formula and mol weight of the used materials.

Material	Full-Name	Mol Weight	Formula	Structure
BMA-1T	4,4'-(2,5-Thiophendiyl)bis[N,N-bis(4-methylphenyl)benzolamin]	626.85	$C_{44}H_{38}N_2S$	
BMA-2T	4,4'-(2,2'-Bithiophen-5,5'-diyl)bis[N,N-bis(4-methylphenyl)benzolamin]	708.26	$C_{48}H_{40}N_2S_2$	

BMA-3T	4,4'-(2,2':5',2''-Terthiophen-5,5''-diyl)bis[N,N-bis(4-methylphenyl)benzolamin]	791.10	$C_{52}H_{42}N_2S_3$	
BHA-1T	4,4'-(2,5-Thiophendiyl)bis(N,N-diphenylbenzolamin)	570.74	$C_{40}H_{30}N_2S$	
BHA-2T	4,4'-(2,2'-Bithiophen-5,5'-diyl)bis(N,N-diphenylbenzolamin)	652.87	$C_{44}H_{32}N_2S_2$	
BHA-3T	4,4'-(2,2':5',2''-Terthiophen-5,5''-diyl)bis(N,N-diphenylbenzolamin)	734.99	$C_{46}H_{34}N_2S_3$	
BFA-1T	4,4'-(Thiophen-5,5'-diyl)bis[N,N-bis(4-fluorphenyl)]benzolamin	642.71	$C_{40}H_{26}F_4N_2S$	
BFA-2T	4,4'-(2,2'-Bithiophen-5,5'-diyl)bis[N,N-bis(4-fluorphenyl)]benzolamin	724.83	$C_{44}H_{28}F_4N_2S_2$	

22

BFA-3T	4,4'-(2,2':5',2''-Terthiophen-5,5''-diyl)bis[N,N-bis(4-fluorphenyl)benzolamin]	806.95	$C_{48}H_{30}F_4N_2S_3$	
BMOA-1T	4,4'-(2,5-Thiophendiyl)bis[N,N-bis(4-methoxyphenyl)benzolamin]	690.85	$C_{44}H_{38}N_2O_4S$	
BMOA-2T	4,4'-(2,2'-Bithiophen-5,5'-diyl)bis[N,N-bis(4-methoxyphenyl)]benzolamin	772.97	$C_{48}H_{40}N_2O_4S_2$	
BMOA-3T	4,4'-(2,2':5',2''-Terthiophen-5,5''-diyl)bis[N,N-bis(4-methoxyphenyl)benzolamin]	855.10	$C_{52}H_{42}N_2O_4S_3$	
B^{t}BuA-1T	4,4'-(Thiophen-5,5'-diyl)bis[N,N-bis((1,1-Dimethylethyl)phenyl)]benzolamin]	795.17	$C_{56}H_{52}N_2S$	

B^tBuA-2T	4,4'-(2,2'-Bithiophen-5,5'-diyl)bis[N,N-bis((1,1-Dimethylethyl)phenyl)benzolamin]	877.29	$C_{60}H_{64}N_2S_2$	
BTMSA-1T	4,4'-(Thiophen-5,5'-diyl)bis[N,N-bis(4-(trimethysilyl)phenyl)]benzolamin	859.47	$C_{52}H_{62}N_2SSi_4$	
BTMSA-2T	4,4'-(2,2'-Bithiophen-5,5'-diyl)bis[N,N-bis(4-(trimethylsilyl)phenyl)benzolamin]	941.59	$C_{56}H_{64}N_2S_2Si_4$	

Table 3-1: Name, structure, chemical formula and mol weight of the used organic substances.

Furthermore, Tris-(8-hydroxyquinoline)aluminum (Alq3) (CAS-Nr. 2085-33-8) and Lithium Fluoride (CAS-Nr. 7789-24-4) was bought from Sigma Aldrich.

3.2.2 Electrode Materials

As electrode material a metal with a low work function is beneficial as mentioned above. The drawback of such materials with a low work function is the fast oxidation in air. As published in most papers for a single layer device an alloy of magnesium and silver is deposited simultaneously onto the organic light emitting material to achieve a relatively stable material with a low work function. During this work only pure magnesium was used as cathode material for the deposition onto the organic material. For the fabricated devices with Alq3 as emitting layer aluminum was used as cathode material.

3.3 Evaporation Device

A new vacuum deposition device has to be constructed because the thermal evaporation of organic materials pollutes the vacuum deposition chamber where other high accurate process steps for semiconductors are performed. Moreover, the deposition of thin films of magnesium can result in a

fast oxidation of the magnesium films when these films get in contact with oxygen. A draft of the newly constructed chamber is shown in Figure 3.2.
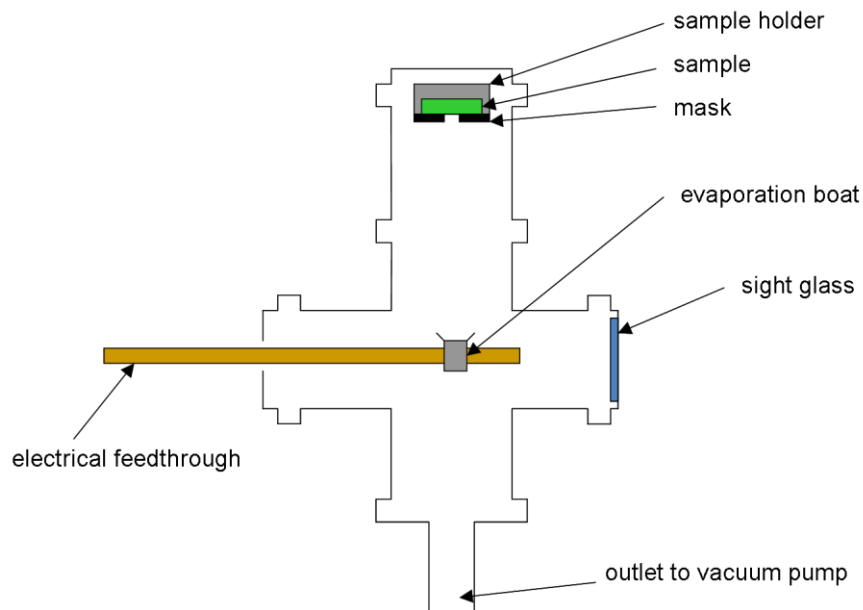
Figure 3.2: Draft of the constructed vacuum chamber.

The new chamber was build out of an ISO-KF system from vacuum parts bought at Trinos. The Tubes and 4-way-cross of the main chamber have a diameter of 50mm to have enough space to mount the sample holder. The vacuum system is pumped by a Pfeiffer vacuum pump to a base pressure of about 10^{-7} mbar. The deposition is carried out by thermal vacuum deposition by means of an electrical feedthrough which can handle 5kVolts and 150 Ampere. The electrical feedthrough is connected to a power source which can provide a current of 30 Ampere.
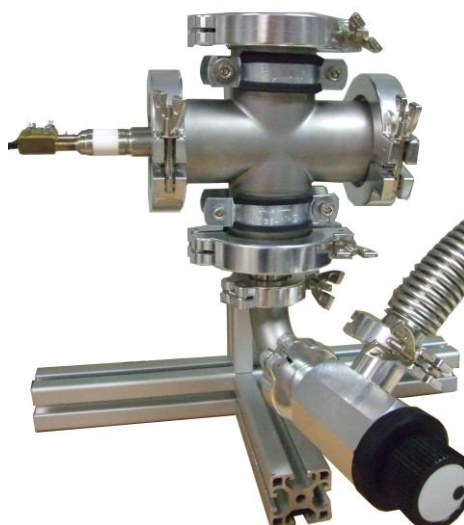
Figure 3.3: Constructed evaporation device.

As evaporation source Molybdenum Boats were bought from Umicore (Nr. 0482047) which can be heated up to about 900°C with a current of 30 Ampere.

With this evaporation chamber it is possible to evaporate the cathode materials as Al and Mg as well as the electron injection layer lithium fluoride (LIF) as shown in Table 3-2. Furthermore, the organic substance Alq3 can be deposited with this device.

Material	Symbol	Melting Point	Evaporation Temperature @ Vacuum Pressure		
			10^{-8} Torr	10^{-6} Torr	10^{-4} Torr
Magnesium	Mg	651°C	185°C	247°C	327°C
Lithium Flouride	LiF	870°C	875°C	1020°C	1180°C

Table 3-2: Evaporation temperature versus vacuum pressure for Mg and LiF.

3.4 Device Fabrication

As mentioned in chapter 2.1 an organic light emitting diode can consist of one or more layers. One layer, the organic light emitting layer, is essential for the operation of the device whereas the other layers are used to enhance the efficiency and therefore the output power of the emitted light.

During this work mainly one layer devices are built with all available organic materials to measure the electro-optical properties of these materials and determine the characteristic properties of the organic

layer. Besides that, a two layer device was built with PEDOT:PSS as hole injection layer to compare the characteristics with the one layer devices.

All devices were fabricated in a clean room environment to avoid the contamination of the sample. The following subchapters provide a detail description of the performed processes.

3.4.1 Cleaning of the substrate

Prior to the deposition of organic and non-organic layers to the ITO covered glass substrate the surface has to be properly cleaned. Therefore the ITO-glass slide was rinsed 1minute in acetone and afterwards 1 minute in isopropanol. Both cleaning steps were performed in an ultrasonic bath for a proper cleaning. After these steps the substrate were dried in stream of nitrogen to get a clean and dry ITO surface for the further deposition steps.

3.4.2 Deposition of the Hole-Injection Layer and the Organic Emitting Layer

For the deposition of the organic emitting layer the most published method is the evaporation of the organic material onto the ITO surface. For organic materials which are solvable in solutions like Toluol, Chloroform or Tetrahydrofuran (THF) another form of deposition is possible, namely spin coating.

If the hole-injection layer PEDOT:PSS is deposited prior to the organic material the surface has to be treated to get an hydrophilic surface. Therefore, the raw ITO-glass slide is treated in oxygen plasma for 1min at 300W in a PlasmaLab device. After the additional cleaning step the water-soluable PEDOT:PSS can be spin-coated onto the ITO surface. The characteristic values for the layer as the spin speed and the associated thickness are discussed in chapter 4.1.2. After spin coating of the PEDOT:PSS the sample is put on a hotplate for 10min at 100°C to evaporate the remaining water and to build a homogeneous layer.

For spin-coating the organic materials which were described above the powdery substances are dissolved in Toluol and filtered with a 0.3nm syringe filter. In a next step 300µl of the solved organic material is spin-coated onto the ITO surface at certain speeds for 30sec on a spin-coater. The variation of the spin-speed results in a variation of the film thickness which will be discussed later.

After the deposition of the organic emitting layer the sample is immediately put into the vacuum chamber for further processing to reduce the risk of contaminations. Furthermore, the remaining solvent of the spin coating process evaporates in the vacuum which results in better characteristics of the organic layer.

3.4.3 Physical Vapor Deposition of Cathode Materials

The organic emitting material has to be contacted on two sides to apply a voltage. These electrodes are used to stimulate the organic material which results in the emitting of light. Until the deposition of the cathode material the organic layer is only contacted by the anode which is the prefabricated ITO on the glass substrate. This ITO electrode is also called the bottom electrode where the light is emitted through.

For the top electrode – or cathode – a solid metal is used with a low work function to improve the electron injection into the organic layer. The deposition of metal can either be carried out by sputter deposition or thermal evaporation.

Sputter deposition has the advantage of a fast processing because of a small vacuum chamber and a high deposition rate. With this method it is only possible to deposit aluminum because of the used sputter device. Besides that the shadowing effects of patterned surfaces are also very high. Experiments were made in a VonArdenne LS 320 S with aluminum at a base pressure of about $2*10^{-6}$ mbar, a working power of $8*10^{-5}$ mbar and a sputtering power of 50W.

Thermal evaporation as another possible deposition method has a longer processing time but offers the possibility to evaporate nearly every material. Moreover, due to the more parallel aligned flight path of the molecules the shadowing effects are less which is beneficial for a structured surface. Experiments were carried out in the vacuum chamber described before in chapter 3.3 at a base pressure of about $1*10^{-6}$ mbar with a molybdenum boat as resistive heater at a current of 30A.

The deposited metal has to be structured during the deposition process because lithographic processes are not possible afterwards due to the organic layer of the device. Therefore, the metal has to be deposited through a shadow mask to get a patterned surface with multiple electrodes. The design and function of this shadow mask as well as the corresponding bracket are described in the following subchapter.

3.4.3.1 Shadow Mask and Sample Holder for Cathode Deposition

For the fabrication of structured metal cathodes the common technology of optical lithography is not applicable due to the lift-off process where the organic layer also gets dissolved in acetone. In respect to that the metal cathode pads have to be structured contactless with the help of a shadow mask. For this purpose a shadow mask as well as a fixture was designed.
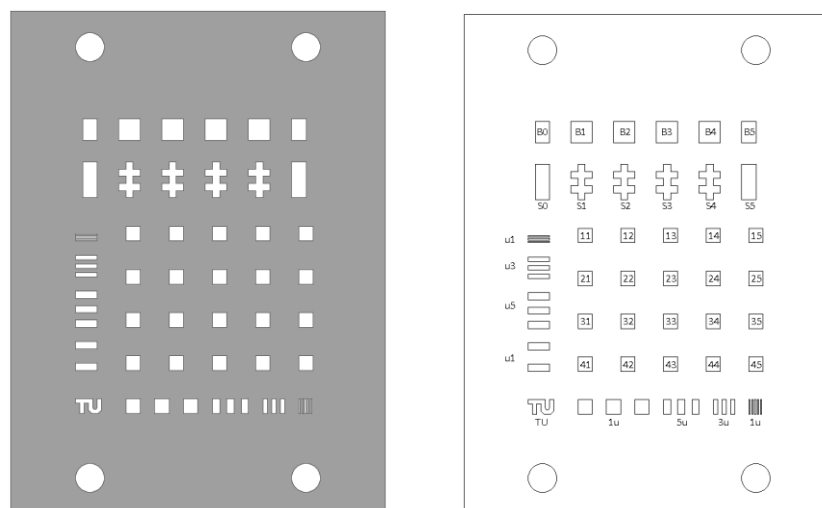
Figure 3.4: (a) Layout of the shadow mask and (b) description of the measurement points

As illustrated in Figure 3.4 the shadow mask consists of numerous rectangular holes as standard cathode as well as other shapes to determine the influence of the area and the circumference of the pad. Two considerations have to be made for defining the size of the pads: the inhomogeneity of the material and the possibility to apply an electrical contact. The spin-coating of the material can result on the one hand in different thickness of the organic layer between the center and the outer regions and on the other hand in the building of nanometer size dots or holes which may produce a short circuit.

Including these considerations the size of the standard cathode metal pads are defined as 1x1mm² (pads 11 to 45 in Figure 3.4b). As mentioned before, other shapes are also designed on the shadow mask. These shapes cover the same area but show a different form and therefore outline to determine if the conduction between the cathode and the organic layer depends either on the area or on the outline of the electrode (pads S0 to S5). Furthermore, small rectangular holes are made on the left side and on the bottom row for electrochemical measurements which are carried out by the Department of Chemistry (pads u1 to u5 as well as pads 1u to 5u).

Because the glass sample has to be put upside down into the vacuum evaporation chamber without touching the shadow mask a fixture consisting of three parts was fabricated.

a)   b)   c)
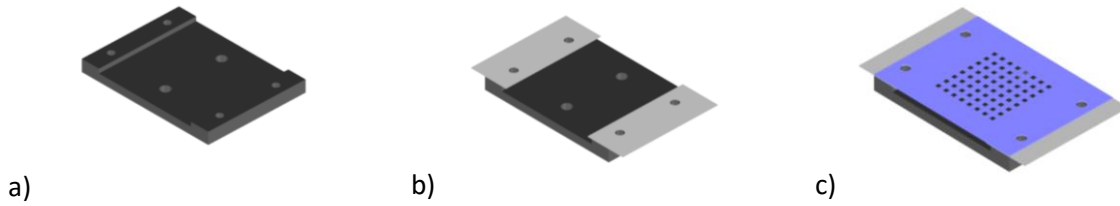
Figure 3.5: Images of the fixture: (a) sample holder, (b) sample holder with distance pads and (c) sample holder with distance pads and shadow mask mounted (screws not pictured).

The lower part of this fixture (Figure 3.5a) is made of aluminum where a 25x25mm² glass slide with a height of 1mm perfectly fits into the cavity in the middle. Two steel distance pads with a thickness of 100nm are put on each side of the bracket (Figure 3.5b) and the shadow mask and the pads are fixed to the bracket with four screws.

The distance pads prevent the shadow mask to touch the sample which otherwise would cause contamination and scratches. Furthermore, the pads are designed as thin as possible to reduce the blurring during the deposition of the metal.

The sample holder was produced by the manufacturing department of the University and the shadow mask was produced by the company Siebtronic in Salzburg. The dimensions of the bracket can be found it the drawings below.
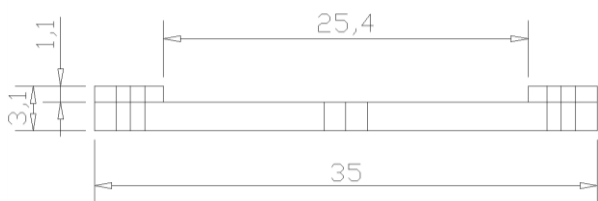
Figure 3.6: Upright projection of the sample holder.
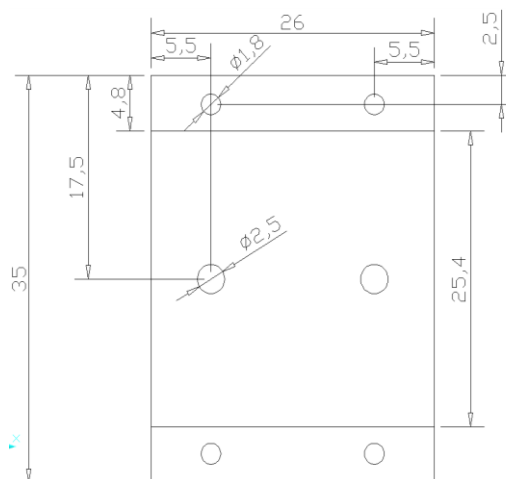
Figure 3.7: Horizontal projection of the sample holder.

The bracket was specially made for square glass slides ordered at Sigma Aldrich with the order number 703176, 703192 or 703184. All of these slides are square with a side length of 25mm and a height of 1.1mm. The difference between the slides is the surface resistivity which alters from 100Ohm/sq down to 8Ohm/sq. For this work the slides with 70-100Ohm/sq are used (Nr. 703176).

3.5   Characterization Methods

For the determination of the electrical, mechanical and optical properties several characterization methods are applied. The results of the different methods are compared to give a comprehensive characterization of the used materials and methods. These methods include electro-chemical methods such as cyclic voltammetry, optical methods such as photoluminescence measurement but also electrical measurements as well as methods with direct mechanical contact to the fabricated device like atomic force microscopy.

3.5.1 Cyclic Voltammetry

A common method to obtain the energy levels and therefore the electrical properties of novel organic conductive materials is the cyclic voltammetry. As mentioned in chapter 2.2.1 the measurement setup consists of a reservoir which contains the organic material dissolved in a solution with conductive salt. Furthermore, the three electrodes are dipped into the water and connected to the measurement device. The setup is illustrated in Figure 3.8 where the counter electrode is positioned on the left side, the working electrode in the middle and the reference electrode on the right side. To reduce the interaction of the reference electrode with the actual measurement the reservoir with the reference is separated by a very small capillary.
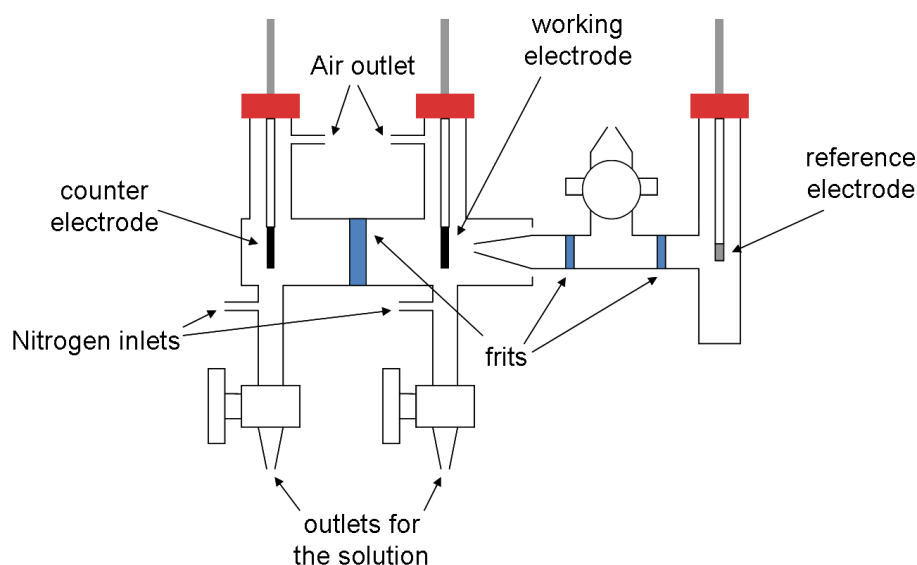
Figure 3.8: Schematic of the cyclic voltammetry device.

For this work all used organic materials were dissolved at a concentration of 0.5mM dm^{-3} in a solution of Dichlormethane and conductive salt. Ammonium tetrafluoroborate at a concentration of 0.1M dm^{-3} was used as conductive salt for the measurement. Prior to every measurement the instrument is calibrated with ferrocene to get the reference potential which is described in many publications to

calculate the desired potential values. If more measurements with different organic substances are done the reference solution is measured again to ensure consistent characteristics of the device. Between the measurements of different substances the chamber was depleted and thoroughly rinsed with acetone. Subsequently the measurement cell was dried in a stream of nitrogen to get a clean environment for the next measurement. If some uncommon spikes or peaks at a reference measurement appear the whole chamber and the fittings have to be clean again carefully to ensure a proper function.

During the measurement it is important to have a proper connection of the fluid between the working electrode, the counter electrode and the reference electrode. Therefore, a Peleus ball is used to fill the chamber which connects the main chamber with the reference electrode. It is important that as much air as possible is sucked out and the chamber is completely filled with the solution to get good conductivity to the reference electrode. Prior to the actual measurement the main chamber (left side) is flushed with nitrogen through the nitrogen inlets to get out the remaining air. During the experiment the solution should not be moved or flushed with nitrogen to prevent a falsification of the diffuse layer and therefore a corruption of the measurement.

For this work the cyclic voltammetry was carried out with a speed of 50mV/sec with two full cycles to eliminate measurement errors of only one cycle which can appear because of transient effects. The reversal points of the sweep voltage were individually adjusted for the different solutions from -1V for the negative reversal point to 2,2V for the positive reversal point.

As mentioned above the cell has to be calibrated with a known solution prior to every measurement. During this work the cell was filled with 0,5mM/dm³ of ferrocene solved in dichlormethan and the conductive salt Ammonium tetrafluoroborate at a concentration of $0.1M$ dm^{-3}. Afterwards 2 cycles with a voltage sweep from -0.4V to 1,4V were carried out to obtain the characteristic graph of the material. The first peak – which represents an oxidation reaction and therefore the HOMO level – can be referred to the known value of -4.8eV against vacuum level. Furthermore, this value can be used to calculate the HOMO levels of the unknown substances.

3.5.2 Photo-absorption Measurement

For a full characterization of a new organic emitting material not only the HOMO level has to be determined, also the band-gap and therefore the wavelength of the absorbed and emitted light has to be measured. The emitted wavelength of the new substances is crucial for an OLED device because it determines the color of the emitted light.
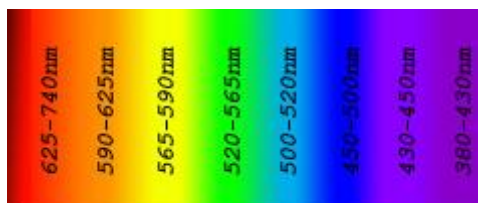
Figure 3.9: Schematics of the color-spectrum of visible light

The measurement was carried out with a Perkin Elmer Lambda 900 Spectrometer. This device is able to cover the full spectrum of ultra violet (UV) and visible light (Vis) which enable the device to emit light at wavelengths from 185nm to 900nm. During this work the characterization was done with a wavelength range of 800nm to 250nm.

The instrument used has a dispersing element and aperture to select a single wavelength before the light passes through the sample cell (see Figure 3.10). With the wavelength dependent aperture it is possible to scan a large range of wavelengths and detect the absorption value for each wavelength separately.
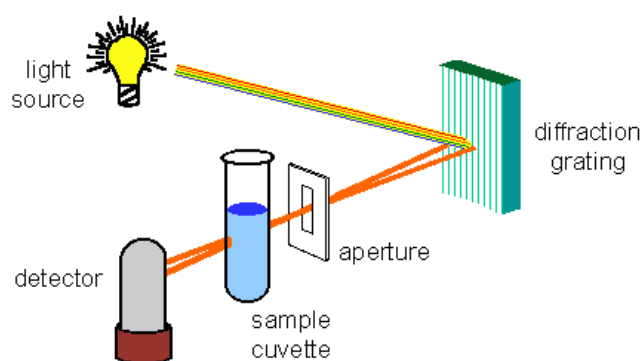
Figure 3.10: Schematic design of the UV-Vis spectrometer.[19]

The measurement can be made with solid substances as well as liquid substances. Because the used materials are all powdery the measurements are carried out with the solid substance fixed between two special glass slides which can be mounted in the spectrometer.
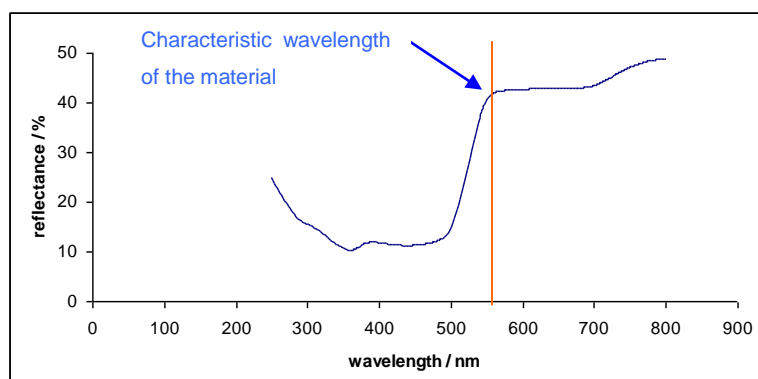
Figure 3.11: Determination of the characteristic wavelength – and therefore the band-gap - of the investigated material.

The spectrometer is parameterized to do a wavelength sweep from 800nm to 250nm. A graph for the measured reflectance of the material is outputted. At the bend between lower absorption and higher absorption of the resulting graph the characteristic wavelength of the material can be determined (Figure 3.11). Hence, the band-gap of the material can be calculated with formula (3-1 whereas h is the Planck constant, c is the light speed and λ is the wavelength.

$$E = h \cdot \frac{c}{\lambda}$$

(3-1)

With the characteristic values of the HOMO level which is obtained by cyclic voltammetry and the band-gap which is obtained with UV-Vis spectroscopy the LUMO level can be calculated. The LUMO level is composed of the energy level of the HOMO level plus the energy of the band-gap.

$$E_{LUMO} = E_{HOMO} - E_{BG}$$

(3-2)

These two energy levels are crucial for the electrical and optical properties of the material because they define the electrical interaction with other materials and the color of the absorbed light. The energy levels define which electrode material best fits for an OLED device.

With the UV-Vis-spectroscopy only the reflection and absorption of the investigated material is characterized. To determine the color of the emitted light a photoluminescence measurement has to be made which is described in the next chapter.

3.5.3 Photoluminescence Measurement

The photoluminescence measurement is used to measure the absorption and emission spectrum of a substance. Therefore the substance is optically stimulated with photons of short wavelength to emit

light of higher wavelength. This measurement was carried out with an Edinburgh FLS920. The substances are solved in THF during the measurement.

The measurement was done in two steps. In the first step the measurement instrument emits photons at different wavelength to detect the maximum of absorption of the investigated substance.

In the second step a fixed emitting wavelength is emitted which is similar to the measured maximum of the absorption from step one. The emitted light from the instrument stimulates the substance under test which starts to emit light. The spectrum of the emitted light of the substance can then be recorded by the analyzer. Therefore, the spectrometer sweeps through a range a wavelength which must be shorter as the stimulation wavelength. For each wavelength the photons are counted by a photon multiplier tube and the maximum peak in the spectrum indicates the characteristic wavelength of the investigated substance.

With this measurement method it is possible to determine the absorption and emission spectrum of the substance. The obtained data can be used to calculate the Stokes shift as well as the band-gap. Furthermore, the maximum of the emission spectrum defines the color of the emitted light.

3.5.4 Electrical- and Electro-Optical-Measurements

In the previous described characterization methods the substances are only optically or electrochemically investigated. To determine the electrical and electro-optical properties of the organic substances they have to be electrically stimulated. For the stimulation the organic layer is contacted by two electrodes. Therefore, a simple device has to be fabricated where the organic material is solved in Chloroform, spin-coated onto an ITO-glass slide and covered with a metallic top electrode as described in chapter 3.4.

After the fabrication of the simple OLED device the electrodes are contacted to applied voltage and measure the current and light output. Thus, the device was put into a needle-prober. The ITO-bottom-electrode was contacted with needle which lance beside a pixel of the top electrode through the organic layer directly onto the ITO. The horizontal distance between the bottom contacting and the top-electrode-area is about 1mm to prevent unnecessary losses because of the ITO electrode.

The top-electrode which is made of magnesium or aluminum is contacted with a special fabricated tip. Therefore, a very thin gold wire of about 100µm was wrapped around the tip of a needle (as shown in Figure 3.12) and glued to the tip with conductive silver.
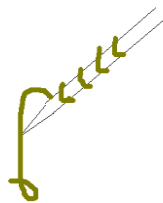
Figure 3.12: Schematics of the modified needle to contact the thin metal top electrodes.

To measure the current-voltage-characteristic the modified tip was softly put in contact with the surface of the top-electrode. With both electrodes contacted it is possible to measure the electrical characteristics (Figure 3.13). Therefore, a voltage sweep was set which starts at 0V and increases up to 30V depending on the type and thickness of the organic layer. To prevent a breakthrough a current limitation is set to 10mA. For a 1x1mm² electrode this would be equivalent to a current density of 10mA/mm².
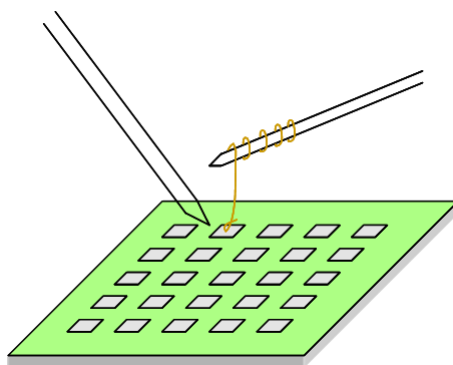
Figure 3.13: Scheme of the electrical characterization of the OLED device.

For the characterization of the electro-optical properties a photo-detector was build and mounted below the OLED cell. The photo-detector consists of a photodiode (model TEMD5010X01 from Vishey, ordered at RSComponents) which is able to detect a wide range of wavelengths from 430nm to 1100nm. The photodiode was connected with a simple circuit (Figure 3.14) to a low noise amplifier which amplifies the signal 100.000 times.
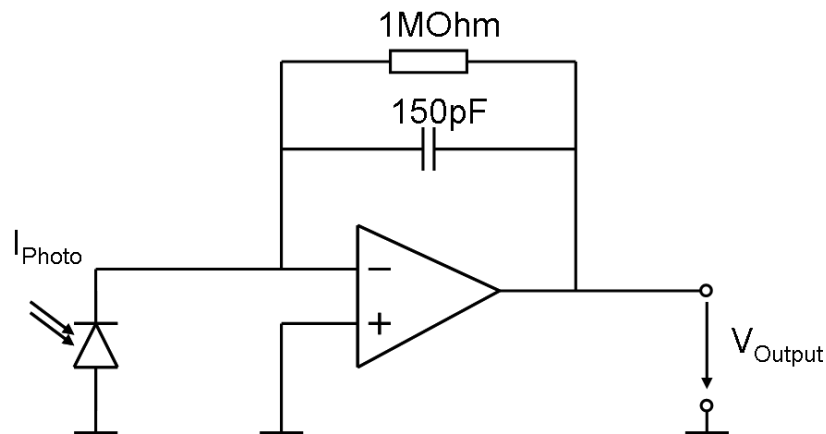
Figure 3.14: Circuit to amplify the current from the photodiode.

Therefore, the luminescence can be calculated from the output voltage of the amplifier.

$$I_{photo} = \frac{V_{output}}{100000 \cdot S(\lambda)} \qquad \text{(3-3)}$$

It the equation above I_{photo} is the Photocurrent of the OLED device, V_{output} the output voltage of the amplifier and $S(\lambda)$ the wavelength depended spectral sensitivity of the photodiode. The relative spectral sensitivity for a wavelength of about 500nm was for the used diode S(500nm)=0.2.

The voltage sweep was generated by a HP Needleprober. The input signals of the measured current and luminescence are recorded with the same device.

4 Results

In this chapter the results of the performed experiments are presented and discussed. Thereby the feasibility to build an emitting OLED from a new class of substances was investigated.

The used materials were electrochemically analyzed with the help of cyclic voltammetry and optically analyzed by photoluminescence spectroscopy to investigate the HOMO and LUMO energy levels. These levels are important for the carrier injection from the ITO anode and the metal cathode. To achieve the smallest possible energy gap between the organic material and the electrodes the electrode material was adopted or an extra layer was added to improve carrier transport.

The layout of the OLED device as well as the thickness of the various layers was altered to investigate the impact on the electrical function and the luminescence of the device. A major point of a well-functioning OLED is the equal injection of electrons and holes into the emitting material as well as the recombination of these carriers within the organic material.

4.1 OLED Device Fabrication

As mentioned above an OLED device consists of multiple layers of materials with specific properties to emit light respectively to improve the efficiency of the device. During this work different layers were deposited onto the ITO covered glass slide with different process parameters to adjust their thickness and electrical properties. The following chapter discusses the electrical and mechanical properties of the different layers which have to be tested to get a satisfying result.

4.1.1 ITO on Glass

The most used substrate for an OLED device is a glass slide on which the electrodes and organic layers are deposited. To contact the organic material electrically two electrodes are necessary where one of them has to be transparent. For this transparent electrode there are only very few materials which fulfill the requirements whereas the best known material is ITO. This metallic material has a good conductivity and a high work function. Glass slides with ITO can either be made by manually deposition of ITO onto a glass slide or can be bought from commercial suppliers like Sigma Aldrich. The advantage of the self-made ITO layers is the possibility to fabricate a structured layer of the metal. Therefore the deposition parameters of the ITO have to be investigated. Subsequently the properties of fabricated ITO layer has to be characterized and compared with the prefabricated ITO-glass slide.

4.1.1.1 Sputter deposition of ITO

An individual glass slide with ITO can be fabricated by sputter deposition of ITO onto the glass surface. This offers the possibility to make different thicknesses of the metal which result in variable

conductivity and transparency. Moreover, the surface of the fabricated ITO layer features a specific roughness which is essential for the further processing steps. If the roughness factor of the surface is very high it is not very beneficial for the deposition of the organic layer which would not be distributed homogeneously over the whole surface. The differences in the thickness of the organic layer can cause an error or an early breakthrough at the electrical measurements.
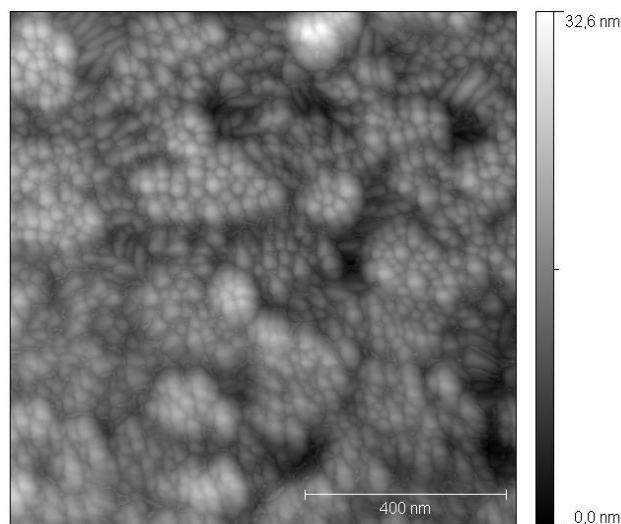
Figure 4.1: AFM image of sputter deposited ITO on a glass slide

The AFM image of the surface with sputtered ITO can be seen in Figure 4.1. These slides have a measured surface roughness of Ra=3.15nm. The roughness was measured on different slides at different positions. The roughness is for all thicknesses of the ITO layer around the roughness of Ra=3nm.

4.1.1.2 Prefabricated ITO on Glass

Prefabricated ITO-Glass slides are available from multiple suppliers which offer a wide variety of sizes of the glass slide as well as thickness and conductivity of the ITO material. The slides of different suppliers show different properties. For this work only the square sized slides from Sigma Aldrich were used with a surface resistance of 70-100 Ohm/sq. For a comparison with the self-made ITO-glass slides the surface roughness of these slides has to be measured.
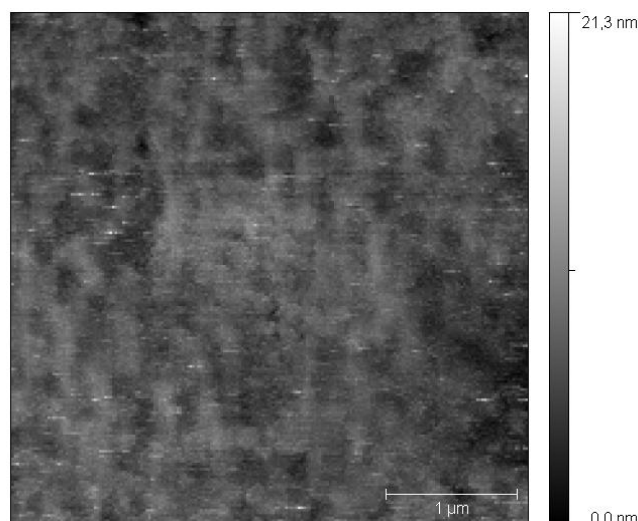
Figure 4.2: AFM image of prefabricated ITO on a glass slide

The recorded AFM image of the surface can be seen in Figure 4.2. With the imaging tool Gwyddion the surface roughness of these slides was determined as Ra=2.4nm. The roughness did not vary much between different slides and different positions on the slide.

4.1.1.3 Comparison of a sputter deposited ITO to prefabricated ITO

The surface of the prefabricated ITO has a lower surface roughness than the ITO fabricated by sputter deposition as shown above. Moreover, the surface looks generally more flat on the prefabricated image. A low roughness is very beneficial for the following spin coating step because a more homogeneous distribution of the material and more flat layer can be expected. Because the conductivity and the roughness factor of the prefabricated ITO glass slides are very constant the prefabricated slides are chosen for further measurements.

4.1.2 Hole Injection Layer

In the previous chapters the properties of the glass substrate covered with an ITO anode are described. Such a substrate offers the possibility to contact the organic emitting material by a transparent electrode. In the following part the properties of an optional layer are described which should enhance the injection of carriers from the anode into the organic emitting material. Additionally, the ITO surface should be flattened by the layer.

For emission of photons electrical charges have to be injected into the organic material which recombines in the layer. A higher recombination number of the charges in the organic layer results in a stronger luminance of the OLED. The number of electrical charges which are injected into the organic layer can be improved by an enhancement of the carrier injection.

To increase the carrier injection from the ITO anode into the organic emitting material a Hole-Injection-Layer (HIL) is deposited on top of the ITO. This HIL has a higher work-function than the ITO but should have a higher work-function than the organic material. This should increase the transfer rate of charge carriers between the organic material and the electrode.
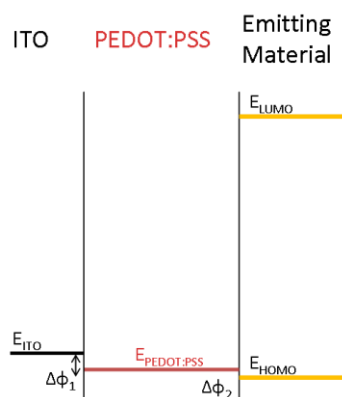
Figure 4.3: Schematic of the energy levels of the junction between the ITO, the PEDOT:PSS layer and the organic material

For this work the material PEDOT:PSS was used as HIL. The work-function of PEDOT:PSS is 5.1eV which is situated in the range of the HOMO level of most of the organic materials which are used in this work. The HOMO levels of these substances are in the range between 4.86eV and 5.38eV. The used procedure to measure these levels are described in chapter 4.2.1.

The use of the HIL additionally offers the benefit that the resulting surface of the spin-coated material is more flat then ITO surface. The flattened surface results in a more homogenous layer of the organic material too.

To achieve the process parameters for the spin-coating process of PEDOT:PSS different process settings were used to deposit the HIL onto prefabricated ITO. Therefore, the spin speeds was altered between 1500rpm and 3000 rpm to get a relationship between the spin-speed and the resulting film thickness. Figure 4.4 shows the graph of the film thickness which varies from 83nm to 108nm.

The thickness of the PEDOT:PSS layer was measured with an AFM. Therefore, a hole was scratched out of the soft material with the AFM tip in contact mode. Afterwards the depth of the hole was measured with the AFM in tapping mode which equates the thickness of the layer.

The faster, contactless investigation of the film thickness with ellipsometery was not possible. The three transparent respectively semi-transparent layers of glass, ITO and PEDOT:PSS have nearly the same refraction index and therefore an accurate measurement was not possible.

spin-speed	thickness
[rpm]	[nm]
1500	108
2000	103
2500	96
3000	83

Table 4-1: Spin-speed to layer thickness dependency of PEDOT:PSS
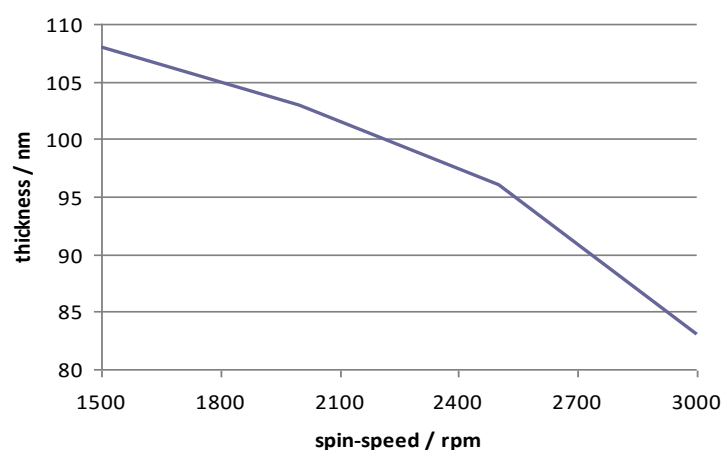
Figure 4.4: Relationship between spin-speed and layer thickness of PEDOT:PSS on ITO

The surface roughness of the PEDOT:PSS layer was also measured during the experiments. It turned out that the roughness stays the same for all spin-speeds at about Ra=0,65nm with a variation of 0,05nm. This value is low compared to the roughness of the clean ITO surface which was about Ra=2,4nm.

Summing up, the deposition of a PEDOT:PSS layer should improve the electrical properties in form of better charge carrier transport. Moreover, the surface roughness is also improved by reduction of the roughness factor from Ra=2,4nm to Ra=0,65nm. Both properties are advantageous for the following deposition of the organic emitting layer. Additional the parameters for the spin-coating process of the material are determined which show that an alteration of the spin-speed between 1500rpm and 3000rpm results in a layer thickness of 108 to 83nm.

4.1.3 Organic Layer

The organic layer is the essential part of an OLED. In this layer the electrons and holes which are injected from the anode and cathode recombine. The recombination of the carriers leads to the emission of light. With the help of hole-injection-layers and electron-transfer-layers it is possible to

increase the light output by improving the charge carrier density. These two layers not only help that more charge carriers are injected into the organic material they also increase the chance that the recombination appears in the organic material instead of at the electrode. Moreover, the type and thickness of the organic material have an influence to the electrical and electro-optical properties of the device.

Therefore, multiple measurements have been made to determine the difference of the thickness of the spin coated material. During these measurement the roughness of the organic surface was also investigated which is essential for the detection of imperfections of the layer. Imperfections like holes in the layer and contaminations are very disadvantageous for the electrical contacting with the cathode material.

The thickness of the organic layer was measured by the same two step process with the AFM as the PEDOT:PSS layer before. In the first step the AFM was put in contact mode operation and a 5x5µm² window was scratched out of the organic material. Thereby, the organic material was shifted to the border of the scratched window. In a second step the AFM was put into tapping mode and an area of 10x5µm² was scanned (Figure 4.5). With this technique it is possible to determine the height difference between the ITO surface and the surface of the organic material.

If more than one layer of soft organic or non-organic material is deposited on the ITO surface the thickness of each layer can be determined. Therefore, the thickness of the "soft" film has to be determined after each deposition step. Out of this the thickness of each layer can be calculated.
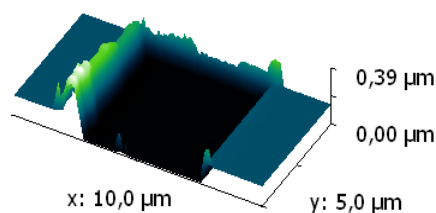
Figure 4.5: 3D AFM tapping mode image of the area where the organic layer was removed.
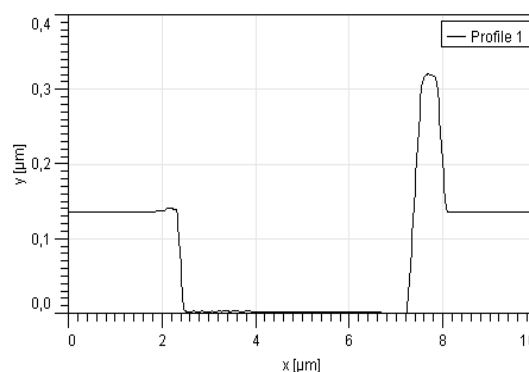
Figure 4.6: Height profile of BMA-1T on ITO at the scratched area.

The spin-speed to thickness dependence was analyzed exemplary for the substance BMA-1T. This substance was dissolved once in Toluol and once in Chloroform. The spin-speed is varied between 1000rpm and 3000rpm. In Table 4-2 the measured values for layer thickness and roughness at different spin-speeds are summarized. The according graphs are displayed in Figure 4.7.

Spin-speed	Toluol		Chloroform	
	Thickness	Roughness	Thickness	Roughness
rpm	nm	nm	Nm	Nm
1000	90	0.23	158	0.17
1500	72	0.22	143	0.15
2000	69	0.25	132	0.22
2500	64	0.23	127	0.17
2800	65	0.25	126	0.18
3500	58	0.26	125	0.15

Table 4-2: Dependency of spin-speed to layer thickness and surface roughness of BMA-1T dissolved in Toluol and Chloroform.

a)   b)
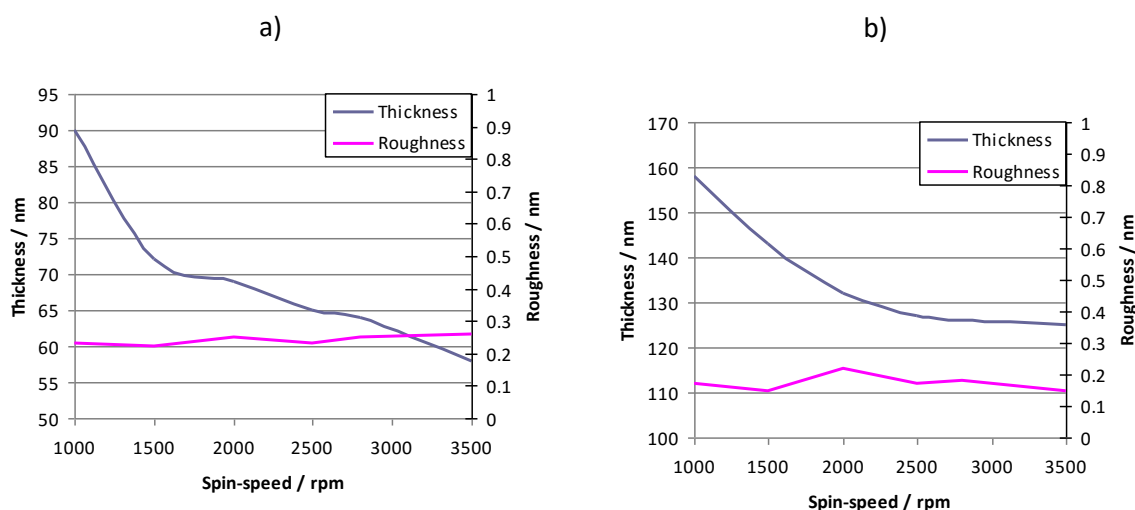
Figure 4.7: Dependency of spin-speed to layer thickness and roughness of BMA-1T dissolved in Toluol (a) and Chloroform (b)

The layer thickness of the organic material has a high dependency on the spin-speed as it can be seen in the measured values above. For BMA-1T dissolved in Toluol it varies between 90nm and 58nm and for the same substance dissolved in Chloroform it varies between 158nm and 125nm. In both cases the same concentration of 20mg/ml BMA-1T was used. The surface roughness on the other side alters only insignificantly at different spin-speeds and is nearly constant around Ra=0.22nm for the Toluol solution and Ra=0.18nm for Chloroform solution.

The thickness and roughness of all substances (BMA-nT, BHA-nT, BTMSA-nT and BtBuA-nT) were analyzed when dissolved in Chloroform and spin-coated at a spin-speed of 2000rpm for 30seconds.

		BMA-1T	BMA-2T	BMA-3T	BHA-2T	BFA-2T	BtBUA-1T	BtBUA-2T	BTMSA-1T	BTMSA-2T	BMOA-1T	BMOA-2T
Thickness	nm	132	135	136	110	124	177	156	179	162	161	168
Roughness	nm	0.22	0.19	0.35	0.19	0.3	0.23	0.24	0.27	0.28	0.21	0.34

Table 4-3: Thickness and roughness of the organic materials after spin-coating with 2000rpm for 30 sec.

As shown in Table 4-3 the thickness of the spin-coated materials differs between 110nm and 179 nm. As written in other publications an optimal thickness for a maximum of emitting light the organic emitting layer should be about 100-150nm in thickness. Therefore the obtained values are around the desired thickness values.

The thickness and roughness for the materials BHA-1T and BFA-1T could not be obtained because of insufficient amount of organic material to run the spin coating and characterization tests. The spin-coating characteristics of BHA-3T could also not be determined because the substance was neither solvable in Toluol nor in Chloroform.

After spin-coating of the organic emitting layer the layer has to be contacted with the cathode to obtain a complete device which can be electrically stimulated.

4.1.4 Cathode

For the electrical stimulation of organic light emitting materials two electrodes are necessary: the anode at the bottom of the material which is usually made of transparent ITO and the cathode at the top which is usually made of a non-transparent metal. The electrical and mechanical properties of the electrodes must fit to the organic material. Many organic materials need a metal with a low work-function to work probably as a simple OLED.
A drawback of metals with a low work-function is usually the high susceptibility to oxidation at air and the reaction with the organic material. Such a suitable metal is for example magnesium which has a low work-function of 3.66eV but also a high oxidation rate on air. An overview of the work-function of various metals which are suitable as cathode material and which are often used in chip fabrication are shown in Table 4-4.

	Mg	Al	Au	Cu	Ag	Li	Na	Ca
description	magnesium	aluminium	gold	copper	silver	lithium	sodium	calcium
work-function	3.66	4.06	5.1	4.53	4.52	2.93	2.75	2.87

Table 4-4: Work-function (in eV) of selected metals.[29] [30]

The metals which are normally used for microelectronic components like Au and Cu have very high work-functions. Metals which are more difficult to process like Li, Ca and Na have low work-functions. The contacting with the cathode material could also be done non-directly by adding an intermediate layer between the metal electrode and the organic layer. Such a two layer electrode enhances the light output of the device because of a better electron injection into the emitting layer and also offers the possibility to use a wider variety of metals as cathode material.
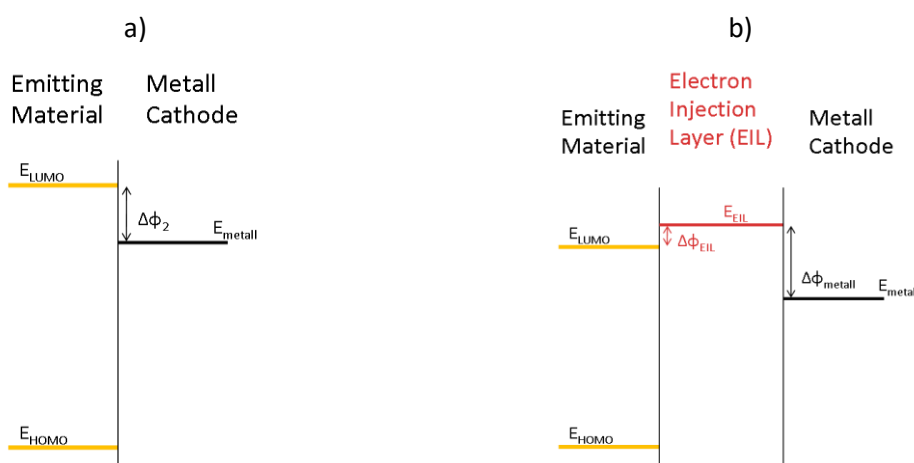
Figure 4.8: Schematics of the energy levels of (a) a basic OLED device and (b) an OLED device with an additional electron-injection-layer.

For this work only simple devices with magnesium as cathode are produced to determine the electrical and electro-optical characteristics of the organic material. The magnesium material is beneficial because of the low work function and easy to handle at normal atmosphere.

Besides the simple devices with only magnesium as cathode there are also multi-layer cathodes were either an electron-injection-layer (EIL) or an electron-transfer-layer (ETL) is used for an improved function of the device. During this work some experiments with Alq3 as ETL as well as with LiF as EIL were carried out. Regarding to other publications the best efficiency for the light output would be achieved with the use of an additional layer of lithium floride (LiF) with a thickness of 3-5nm.

4.2 Material Characterization

The electrochemical and optical characterization of the used substance is important to predict the behavior of the substances. Therefore, the organic base materials were analyzed by cyclic voltammetry to determine the HOMO level of the substance and by photoluminescence to determine the bandgap and hence the wavelength of the emitted light.

4.2.1 Cyclic Voltammetry

The cyclic voltammetry was carried out to determine the HOMO level of the investigated substances which is crucial for the conduction mechanisms of the organic substance and the anode material. The measurement was done with a measuring setup as explained in chapter 3.5.1 by applying a voltage sweep between the working and the counter electrode. The minimum and maximum of the sweep was at least from -0.4V to +1.4V. But these values were altered depending on the material. If the investigated material does not show analyzable results the sweep was adapted to cover a larger voltage area.

At a voltage of about +2.2V all substances showed a strong increase of the current which can be originated from the used solvent. The used solvent dichloromethane is only suitable for the measurement of the positive peak and therefore only for the determination of the HOMO level. For the measurement of the LUMO level the substances have to be solved in THF to show good results with more negative voltages applied to the electrodes.

The resulted diagrams of the measured data of the substances are shown below. From these measured values the HOMO level are calculated. Therefore, the voltage level of the first peak is evaluated and compared to the first peak of the characteristic graph of ferrocene. The HOMO level is then calculated by adding the voltage difference between the first peak of the investigated substance and the ferrocene to the known HOMO level of the ferrocene as shown in Figure 4.9.

$$HOMO_{BMA-1T}: 4.8V + (1,21V - 0,94V) = 5.07V$$
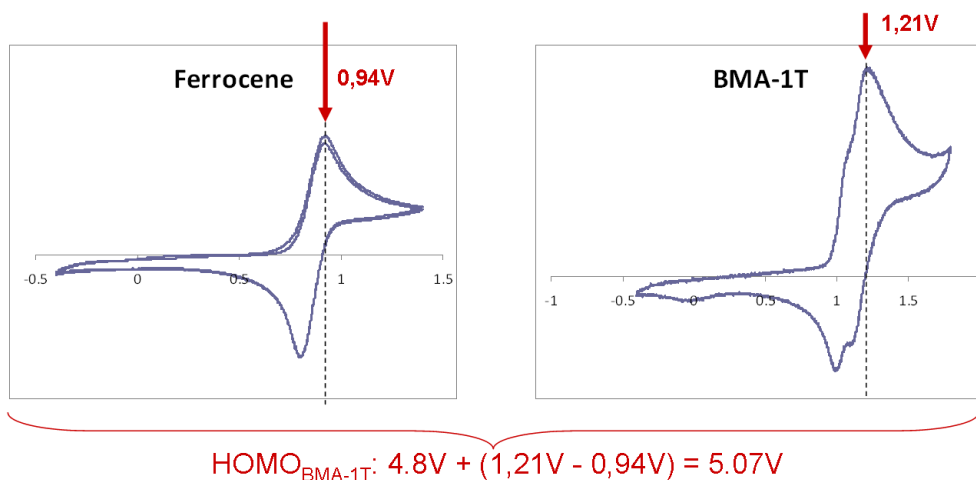
Figure 4.9: Calculation of the HOMO level of a new substance by cyclic voltammetry.

As mentioned in the previous chapters the analysis and conversion of the CV graph is possible due to the comparison to the CV graph of ferrocene. For all measurements a triangle voltage was applied to the electrodes starting at the start potential running up to the upper reverse potential, down to the lower reverse potential and going back to the start potential. This cycle was repeated once.
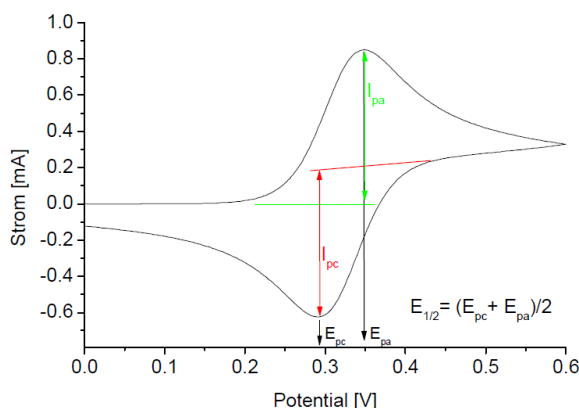
Figure 4.10: Schematic to evaluate the characteristic values of a substance from their voltammetry curves.

The resulted graph can be analyzed to get the cathodic E_{pc} and anodic peak potential E_{pa}. Out of these values the half-wave potential can be calculated with the formula $E_{1/2} = \left(E_{pc} + E_{pa}\right)/2$. Furthermore, the anodic i_{pa} and cathodic peak currents i_{pc} can be measured. The calculation of the half-wave potential is only possible if the CV fulfill three specific criteria which are called reversibility:

1. The difference between E_{pc} and E_{pa} are about 57mV

2. The ratio between i_{pc} and ipa is one

3. V1/2 $\approx$ i, whereas v is the federate and i the maximum current

48

In practice these conditions are hard to fulfill and small aberrations can be tolerated. At fast irreversible reactions of the measured substance the reverse peak disappears. It is the case if the electrochemically generated product is not steady. If the irreversible reaction is not very fast the reverse peak gets only smaller.

It is also possible to get more than one peak because of further reactions of the investigated substances. Some substances can show more than one reaction step which result in more than one current peak. If all chemical reactions which appear during the measurement are reversible the general appearance of the graph, except the multiple peaks, stays the same.[31]

In case of an irreversible reaction the absence of the cathodic peak can be observed. But the current peak of the reverse reaction also depends on the concentration of the substance, the scan rate v, the penetration factor and the amount of the transferred electrons. The absence of the peak for the return reaction is not a significant indicator for an irreversible reaction. The absence could also be caused by a too small concentration of the investigated substance as well as by a consecutive reaction. These consecutive reactions are especially expected in a range of the potential where the solvent starts to dissolve. If the consecutive reactions are reversible the reverse peak can be shown by a decrease of the scan rate.[32]

In the following section all cyclic voltammetry graphs for the investigated substances are shown.
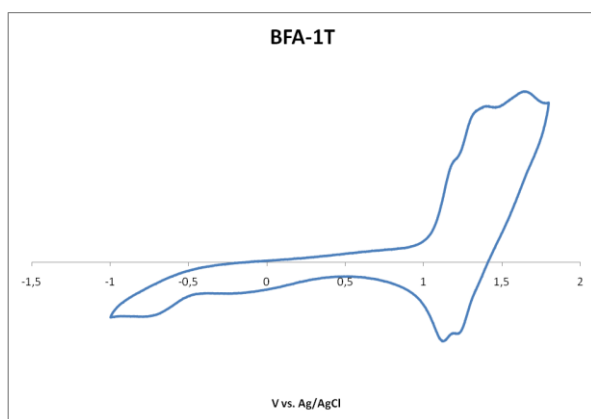
Figure 4.11: Cyclic voltammetry of 0.5mM dm^{-3} of BFA-1T dissolved in a solution of dichlormethane with 0.1M dm^{-3} ammonium tetrofluoroborate.
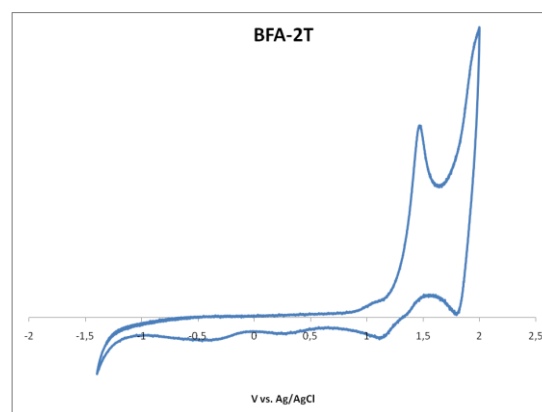
Figure 4.12: Cyclic voltammetry of 0.5mM dm-3 of BFA-2T dissolved in a solution of dichlormethane with 0.1M dm-3 ammonium tetrofluoroborate.
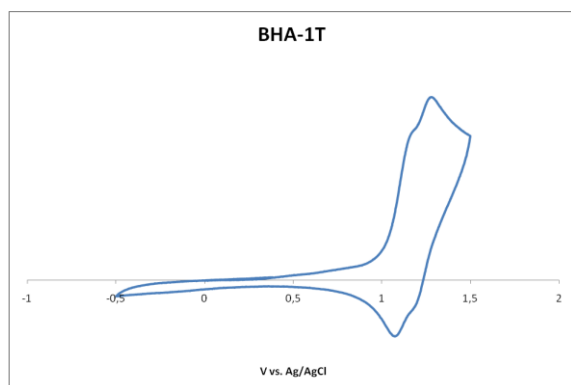
Figure 4.13: Cyclic voltammetry of 0.5mM dm-3 of BHA-1T dissolved in a solution of dichlormethane with 0.1M dm-3 ammonium tetrofluoroborate.
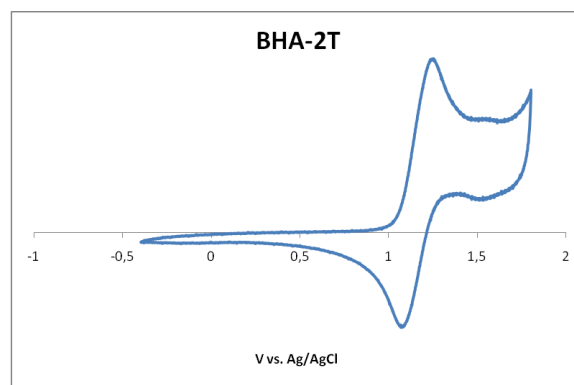
Figure 4.14: Cyclic voltammetry of 0.5mM dm-3 of BHA-2T dissolved in a solution of dichlormethane with 0.1M dm-3 ammonium tetrofluoroborate.
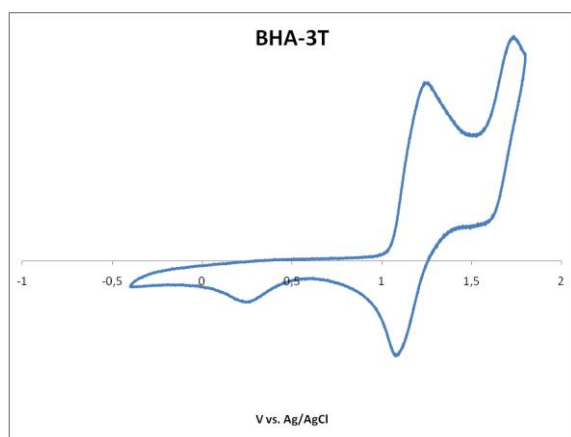
Figure 4.15: Cyclic voltammetry of 0.5mM dm-3 of BHA-3T dissolved in a solution of dichlormethane with 0.1M dm-3 ammonium tetrofluoroborate.
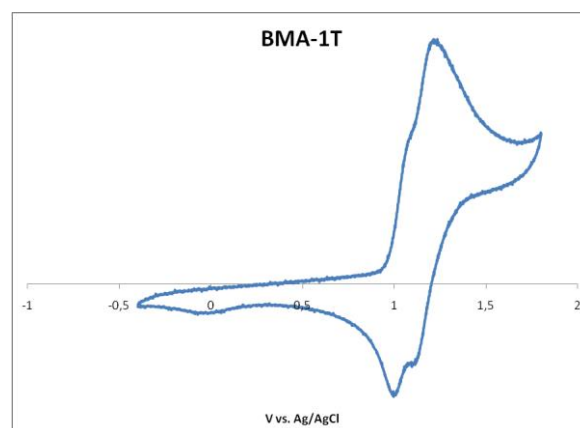
Figure 4.16: Cyclic voltammetry of 0.5mM dm-3 of BMA-1T dissolved in a solution of dichlormethane with 0.1M dm-3 ammonium tetrofluoroborate.
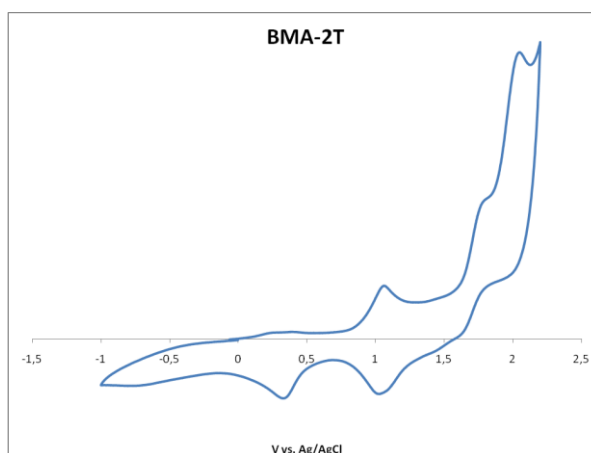
Figure 4.17: Cyclic voltammetry of 0.5mM dm-3 of BMA-2T dissolved in a solution of dichlormethane with 0.1M dm-3 ammonium tetrofluoroborate.
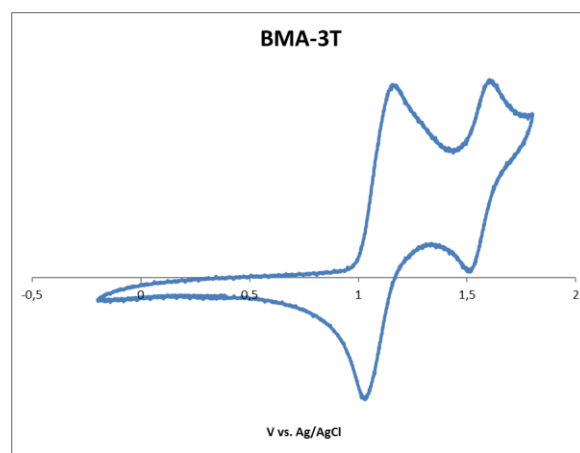
Figure 4.18: Cyclic voltammetry of 0.5mM dm-3 of BMA-3T dissolved in a solution of dichlormethane with 0.1M dm-3 ammonium tetrofluoroborate.
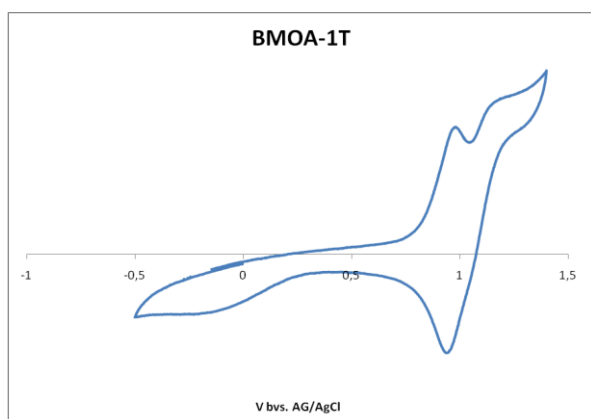
Figure 4.19: Cyclic voltammetry of 0.5mM dm-3 of BMOA-1T dissolved in a solution of dichlormethane with 0.1M dm-3 ammonium tetrofluoroborate.
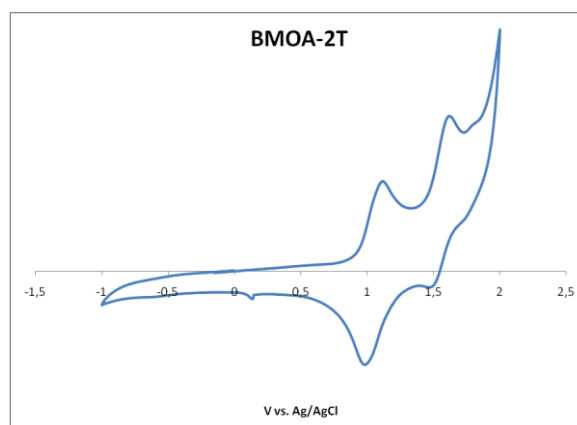
Figure 4.20: Cyclic voltammetry of 0.5mM dm-3 of BMOA-2T dissolved in a solution of dichlormethane with 0.1M dm-3 ammonium tetrofluoroborate.
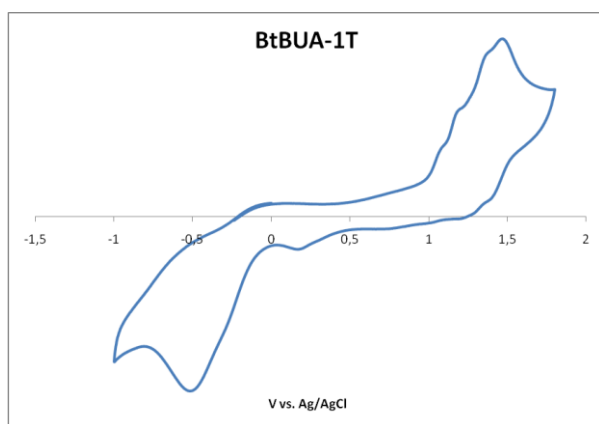
Figure 4.21: Cyclic voltammetry of 0.5mM dm-3 of BtBUA-1T dissolved in a solution of dichlormethane with 0.1M dm-3 ammonium tetrofluoroborate.
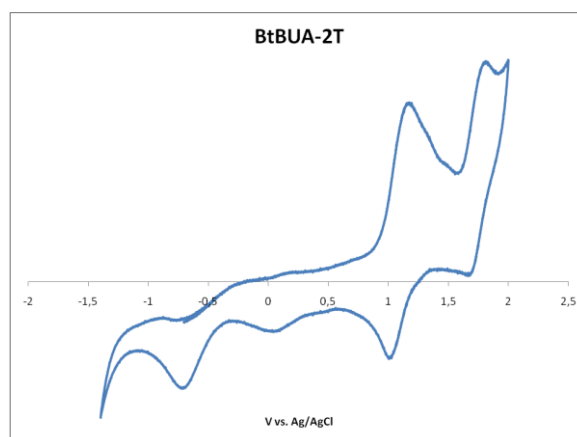
Figure 4.22: Cyclic voltammetry of 0.5mM dm-3 of BtBUA-2T dissolved in a solution of dichlormethane with 0.1M dm-3 ammonium tetrofluoroborate.
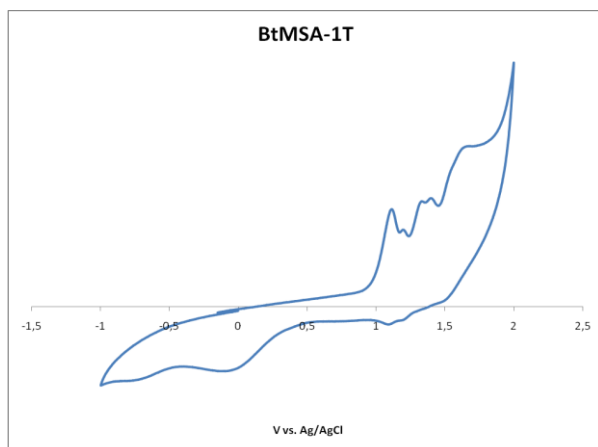
Figure 4.23: Cyclic voltammetry of 0.5mM dm-3 of BtMSA-1T dissolved in a solution of dichlormethane with 0.1M dm-3 ammonium tetrofluoroborate.
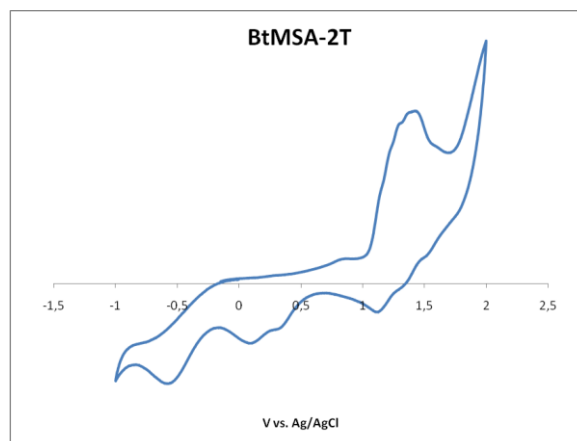
Figure 4.24: Cyclic voltammetry of 0.5mM dm-3 of BtMSA-2T dissolved in a solution of dichlormethane with 0.1M dm-3 ammonium tetrofluoroborate.

The obtained graphs are analyzed as described above to determine the peak values of the first cathodic peak. The potatial of the cathodic peak is compared to the potential of the cathodic peak of ferrocene. The HOMO energy levels to the investigated subtances are calculated as described in formula 4.1.

$$E_{HOMO} = E_{HOMO,ferrocene} + (E_{cp,Substance} - E_{cp,ferrocene}) \qquad \textbf{(4-1)}$$

At this formula E_{HOMO} is the HOMO energy level of the investigated substance, $E_{HOMO,ferrocene}$ the HOMO level of the reference material – in this case ferrocene. $E_{cp,Substance}$ indicates the voltage where the first cathodic peak of the investigated material appears and $E_{cp,ferrocene}$ can be refered to the voltage of the first cathodic peak of ferrocene.

	cathodic peak (Ecp)	ΔE(peak/peakFc)	EHOMO
	V	V	eV
Ferrocene	0.9	0	4.8
BFA-1T	1.33	0.43	5.23
BFA-2T	1.43	0.52	5.32
BHA-1T	1.26	0.40	5.20
BHA-2T	1.25	0.35	5.15
BHA-3T	1.26	0.35	5.15
BMA-1T	1.23	0.31	5.11
BMA-2T	0.95	0.24	5.04
BMA-3T	1.17	0.26	5.06
BMOA-1T	0.96	0.06	4.86
BMOA-2T	1.08	0.21	5.01
BTBUA-1T	1.21	0.36	5.16
BTBUA-2T	1.3	0.39	5.19
BTMSA-1T	1.1	0.22	5.02
BTMSA-2T	1.38	0.47	5.27
H-Star	1.45	0.58	5.38

Table 4-5: Calculated HOMO levels of the organic substances.

The obtained values for the HOMO levels are in the range from 4.86eV to 5.38eV. This results in an energy gap of 0.3 to 0.7eV between the HOMO level of the substances and the work-function of the ITO. For a good conduction between the ITO and the organic material a small energy gap between these materials is beneficial. Therefore, the substances with the lowest HOMO energy level should show the best conductivity which can result in an increased quantum efficiency.

All substances can also be diluted in THF and measured with cyclic voltammetry to get the characteristic values for the LUMO levels. The energy gap between the HOMO and LUMO level can be referred to the characteristic wavelength of the emitted light. But the optical properties such as the characteristic wavelength can also be analyzed by spectrometric measurements.

4.2.2 Spectrometric measurements

To characterize the optical properties of the investigated substances two different measurements are carried during this work. A spectral absorption measurement was done to analyze the maximum absorption wavelength and a fluorescence measurement was done to obtain the wavelength of the emitted light of the material.

4.2.2.1 Optical Absorption of organic light emitting materials

The absorption of the organic materials was measured by exposure of the material to a light source which carried out a wavelength sweep from 800nm to 250nm as described in chapter 3.5.2. For the calibration of the measurement device the empty sample holder was measured to determine the absorption without any substance. Afterwards, the powdery substances are put into the sample holder and the measurement is carried out. The graphs which are recorded during the measurements are used for further analysis.

The characteristic wavelength was determined by analysis of the measured data relative to the graph of the empty sample holder. Therefore, the transmission data of the empty sample holder are subtracted from the data of the organic material. The resulting normalized transmission coefficient should be between 0 and 1. Sometimes the transmission coefficient can be above one because of impurities on the empty sample holder as well as little differences at the mounting of the sample holder. Moreover, a higher coefficient can also be caused by the material which also emits a small amount of long wavelength light.

On the following pages the graphs of the photo-absorption-measurement of the investigated substances are shown.
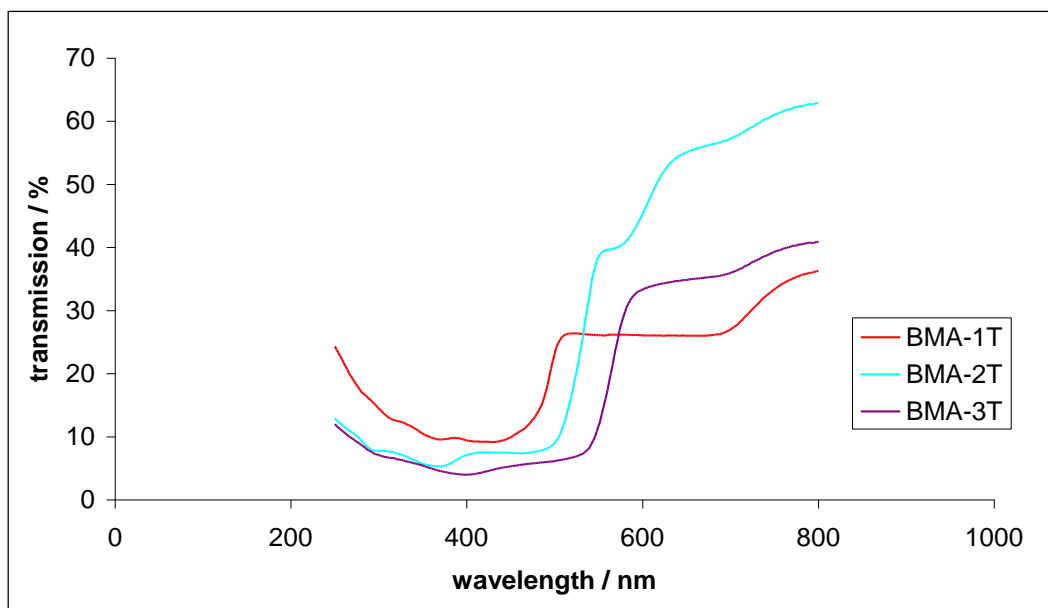
Figure 4.25: Relative Transmission of the organic materials BMA-nT.
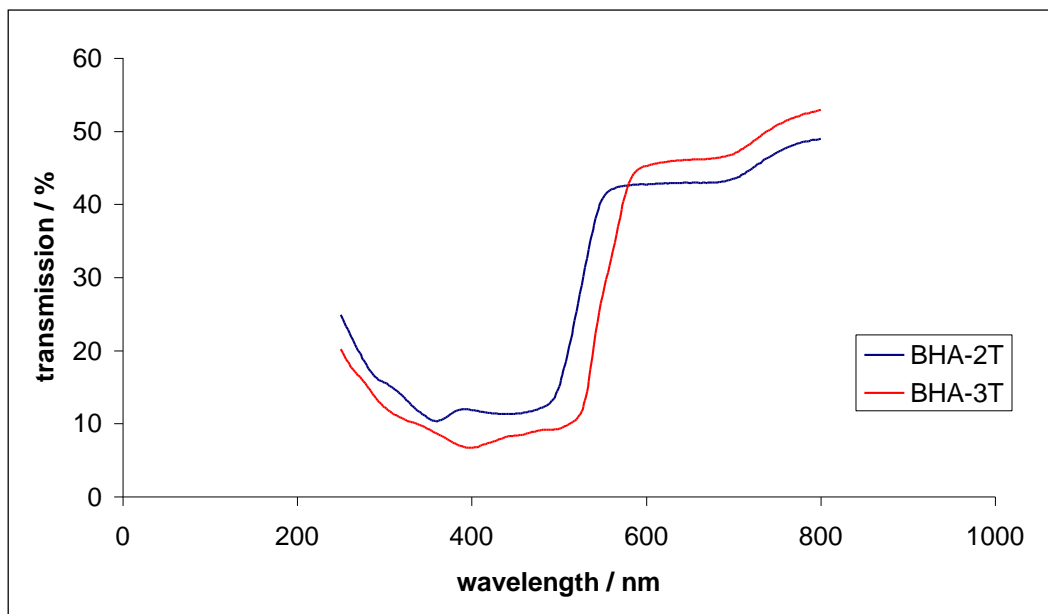
Figure 4.26: Relative Transmission of the organic materials BHA-nT.
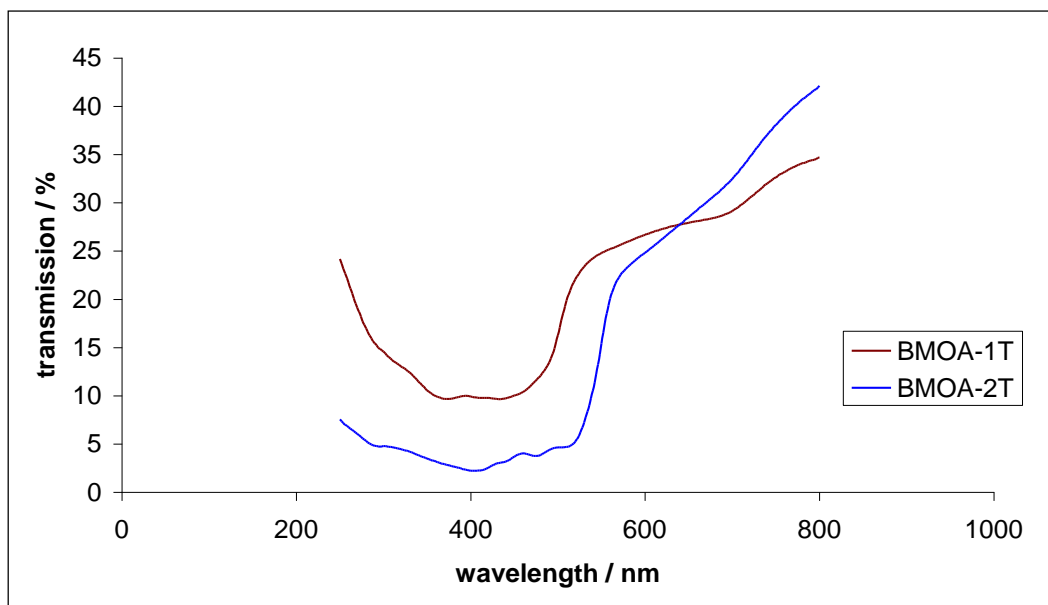
Figure 4.27: Relative Transmission of the organic materials BMOA-nT.
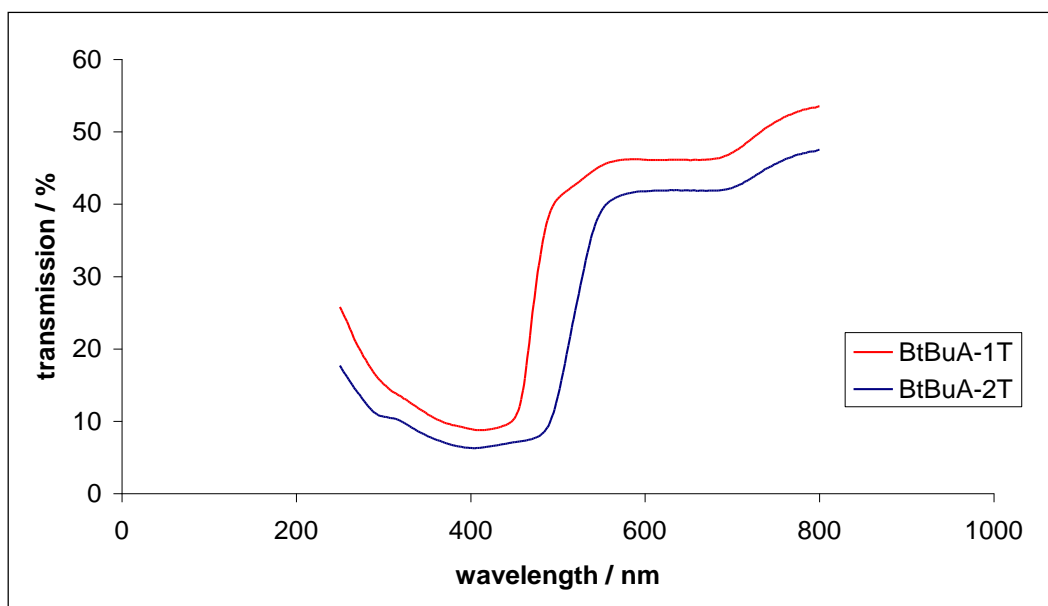
Figure 4.28: Relative Transmission of the organic materials BtBuA-nT.

57
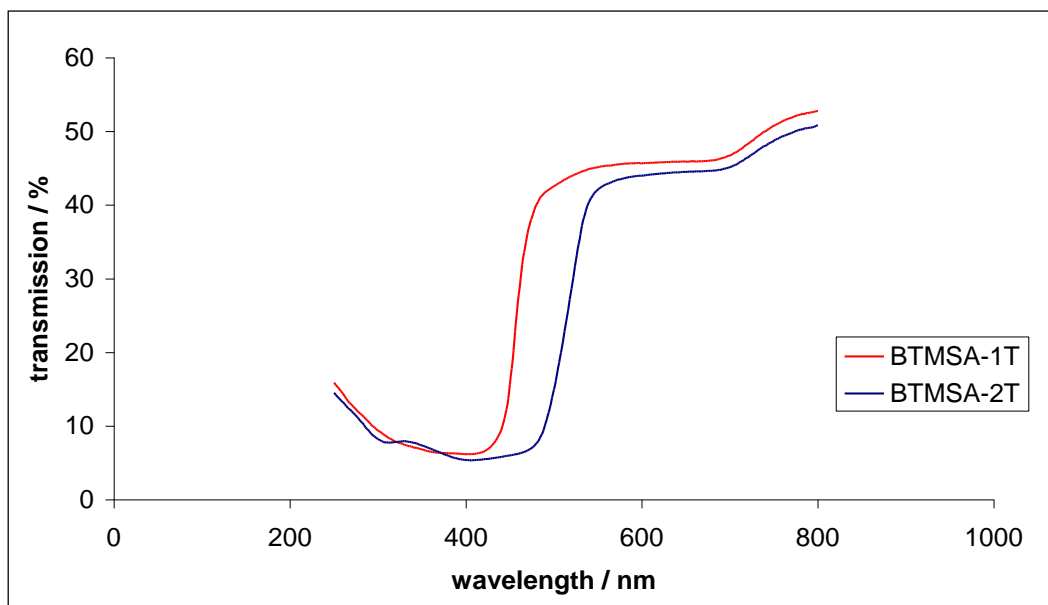
Figure 4.29: Relative Transmission of the organic materials BTMSA-nT.
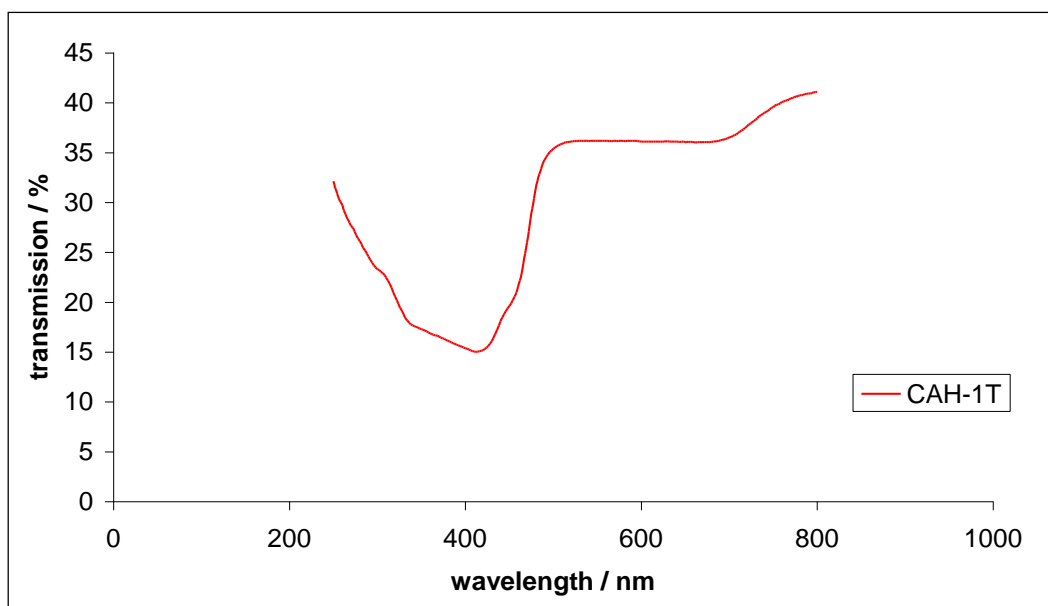
Figure 4.30: Relative Transmission of the organic materials CAH-1T.

The measured absorption values of all substances are analyzed to obtain the absorption wavelength. In Table 4-6 the values are summed up and the obtained wavelength is referred to the photon energy of the absorbed light with formula 4-2.

58

$$E = h \cdot \frac{c}{\lambda}$$

<div align="right">**4-2**</div>

The characteristic wavelength is determined by analyzing the graphical data (as described in chapter 3.5.2). At the bend between the lower absorption and higher absorption of the material the characteristic wavelength of the material can be read off. Light with higher wavelength than the characteristic wavelength is not absorbed because these photons have too less energy to interact with the material and can pass through it with less or no absorption.

material	wavelength	Photon energy
name	nm	eV
BMA-1T	515	2.41
BMA-2T	554	2.24
BMA-3T	602	2.06
BHA-2T	553	2.24
BHA-3T	584	2.12
BFA-2T	548	2.26
BtBUA-1T	560	2.22
BtBUA-2T	586	2.12
BTMSA-1T	554	2.24
BTMSA-2T	564	2.20
BMOA-1T	536	2.32
BMOA-2T	570	2.17
CAH-1T	512	2.42

Table 4-6: Wavelength of the absorption maximum of the organic substances.

The absorption wavelength of the substances BHA-1T and BFA-1T could not be determined because there was too less of the substance available to carry out a proper analysis.

The wavelength of the investigated materials varies between 512 and 586nm. The color spectrum of these substances is therefore in the range of green to light red light. Because of the red shift (Stokes shift) of the emission spectrum the emitted light of these material will be also have a green respectively light red color. On the other hand gives the absorption of photon no information of the possible emission of photons. The absorption wavelength is necessary for the calculation of the HOMO and

LUMO energy levels of the substance. For a more accurate result the substance are also analyzed by photoluminescence measurement.

Photoluminescence measurement

The Photoluminescence measurement of a material gives exact information about the optical absorption and emission properties of the investigated substances. Because these measurements were done with the substances dissolved in THF solvent the measured values differ from the previous UV-Vis measurements which were done with the solid powder of the substances. As described in the experimental part in chapter 3.5.3 two characteristic values are determined by photoluminescence measurement: the maximum of absorption and the maximum of emission.

For the determination of the maximum of excitation the detector energy is locked to a certain value so only photons with one defined wavelength are detected. Afterwards the substance is irradiated by light of different wavelengths which sweep from 250nm to about 500nm. At the maximum of excitation the most photons of the previous defined wavelength are emitted

For the measurement of the maximum of emission the spectrometer is adjusted to detect photons of a wide range of wavelengths by sweeping through a range of wavelength. Thereby, the lower wavelength limit is defined by the previous maximum excitation wavelength. The lower limit has to be a little bigger than the maximum excitation wavelength. Otherwise the PMT will overload because of too many photons and will need a long time to cool down again.

Below the graphs for measuring the excitation and emission spectrum of the investigated substances are shown. The graph for the determination of the excitation maximum is at the side of smaller wavelengths and the graph for determination of the emission maximum on the side of longer wavelengths.

(a)

(b)

(c)
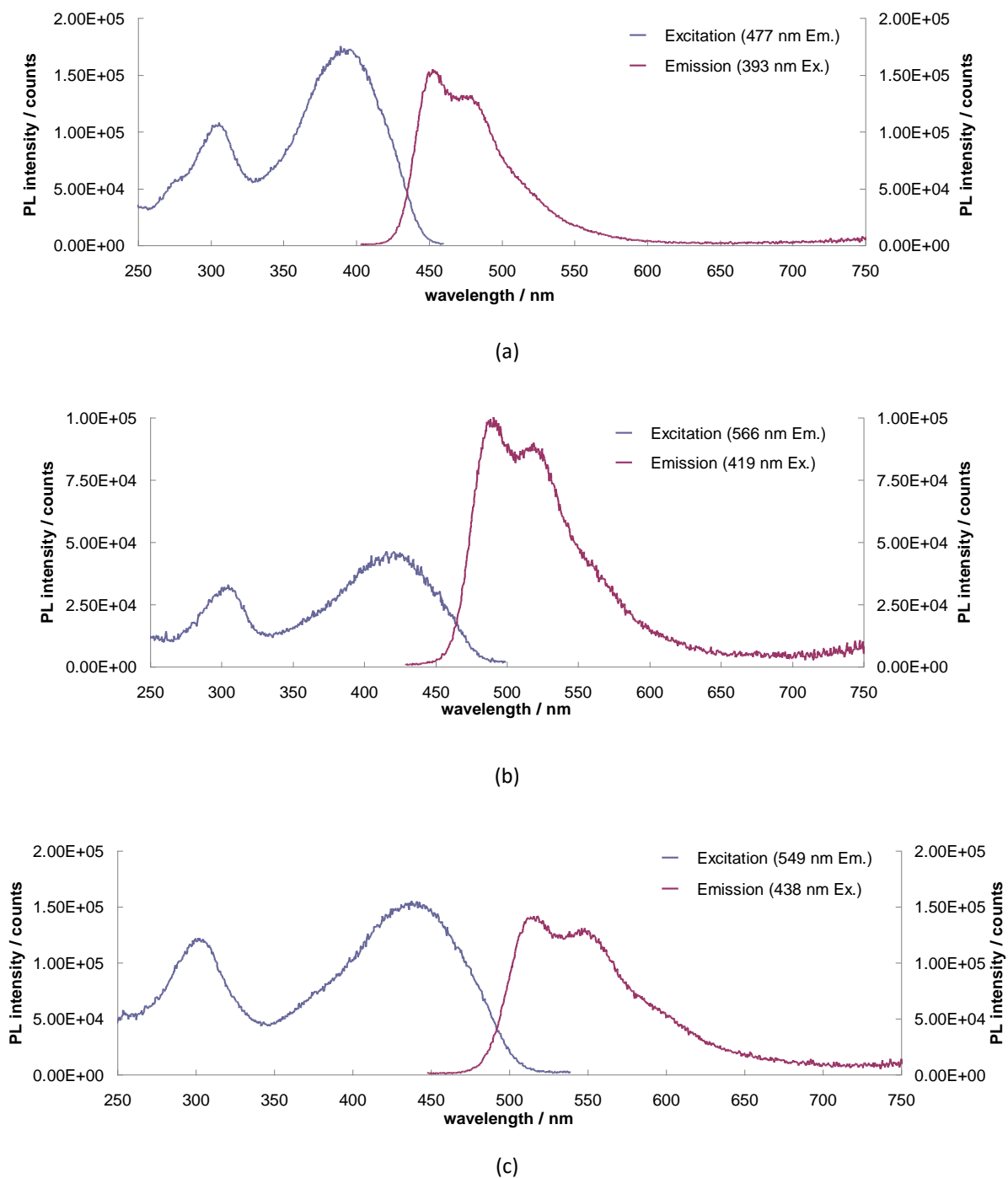
Figure 4.31: Absorption- and emission spectra of (a) BMA-1T, (b) BMA-2T, (c) BMA-3T. For the excitation wavelength of the photoluminescence the respective absorption maxima are used.
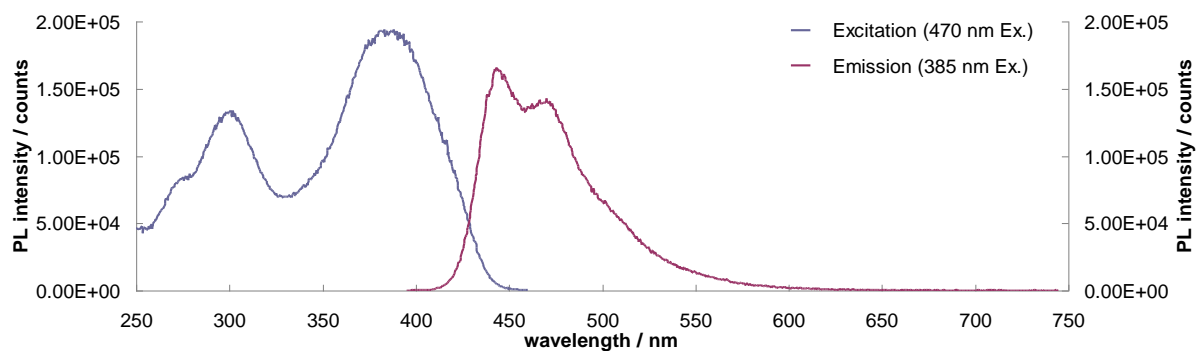
(a)
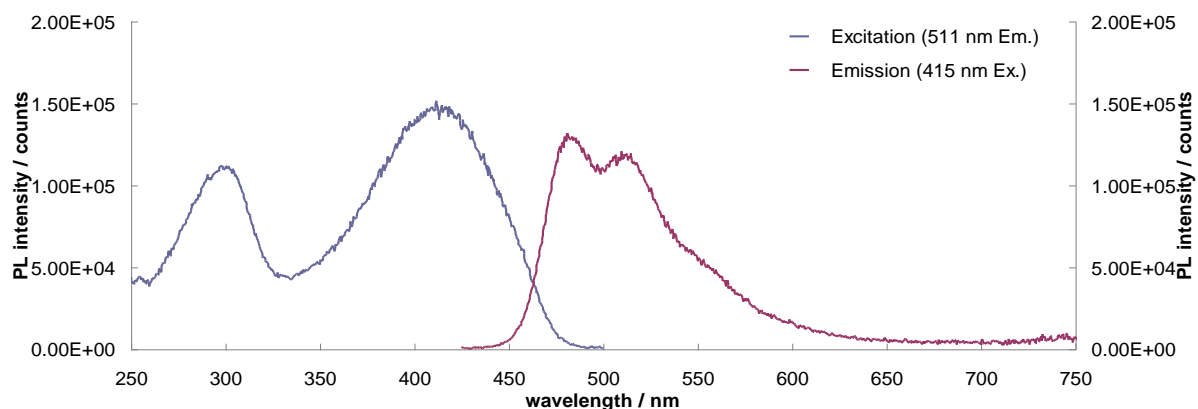
(b)
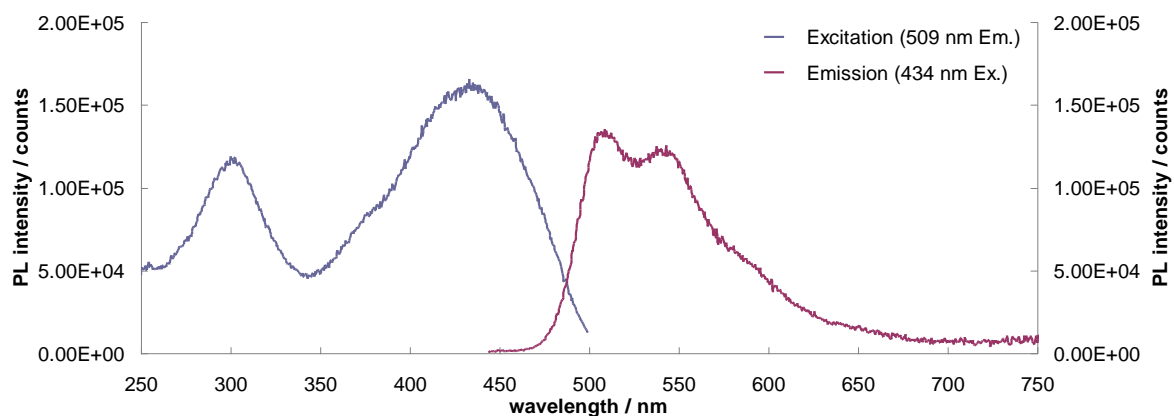
(c)

Figure 4.32: Absorption- and emission spectra of (a) BHA-1T, (b) BHA-2T, (c) BHA-3T. For the excitation wavelength of the photoluminescence the respective absorption maxima are used.
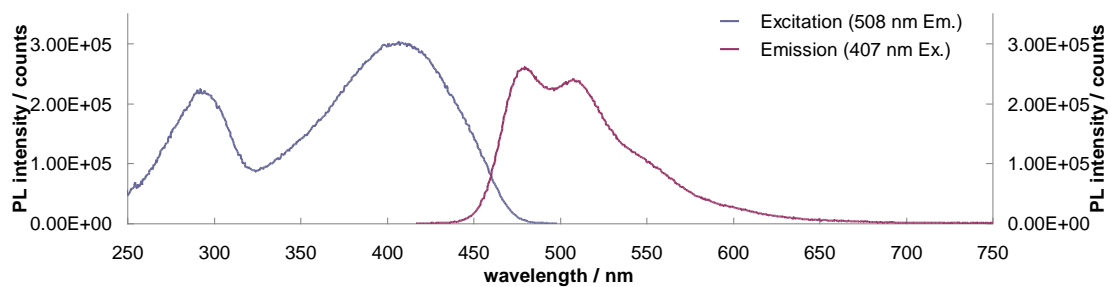
(a)
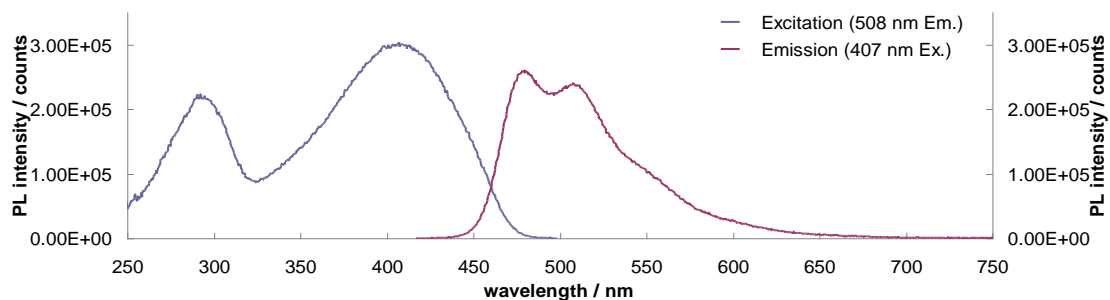
(b)

Figure 4.33: Absorption- and emission spectra of (a) BFA-1T, (b) BFA-2T. For the excitation wavelength of the photoluminescence the respective absorption maxima are used.
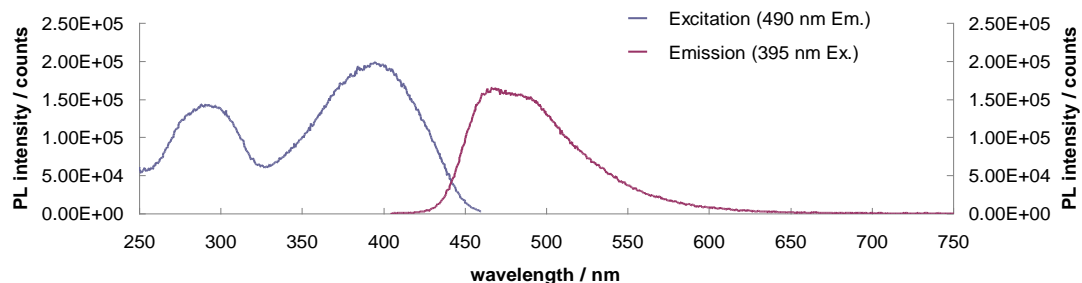
(a)
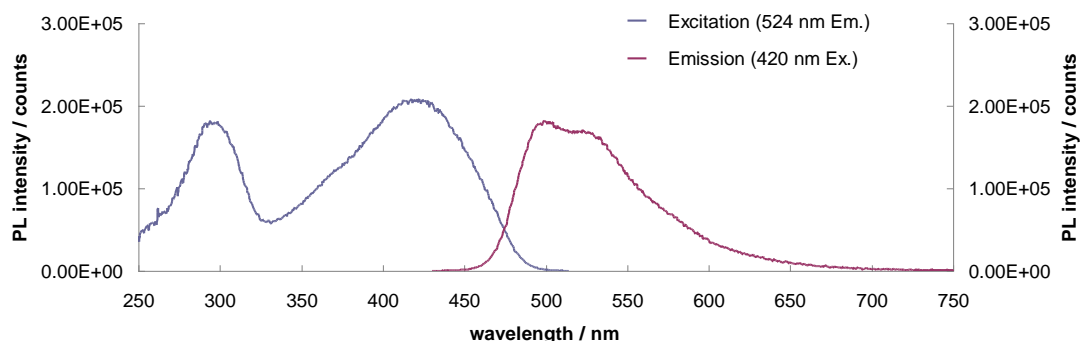
(b)

Figure 4.34: Absorption- and emission spectra of (a) BMOA-1T, (b) BMOA-2T. For the excitation wavelength of the photoluminescence the respective absorption maxima are used.

(a)

(b)
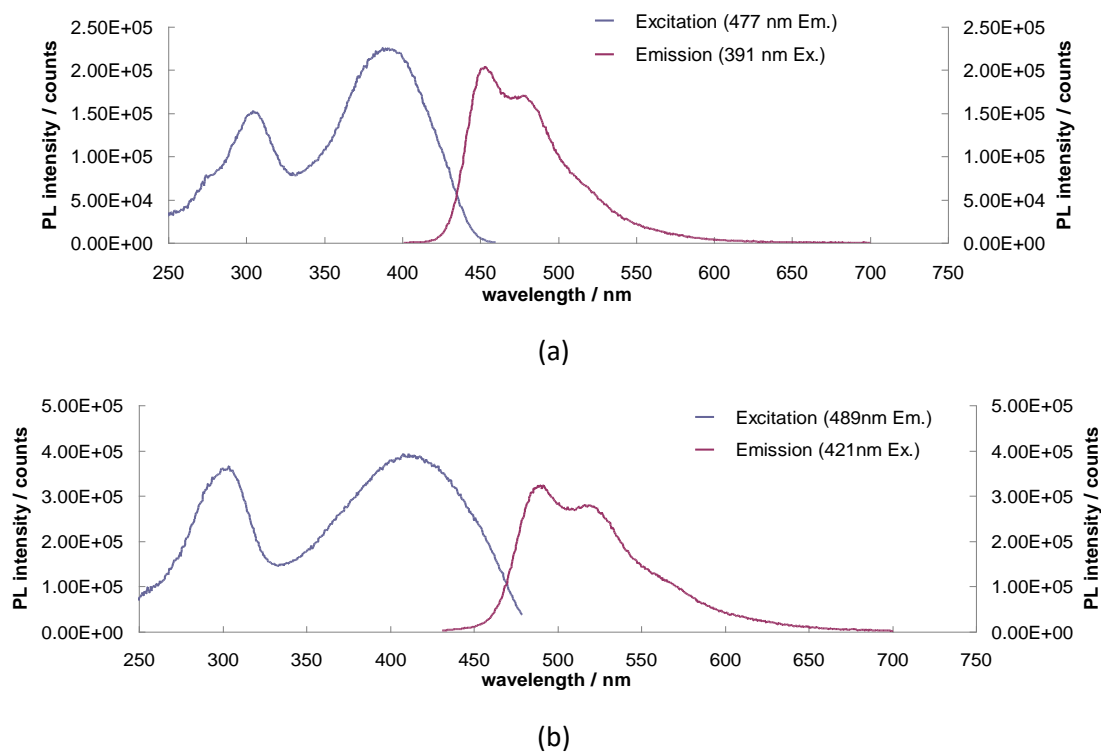
Figure 4.35: Absorption- and emission spectra of (a) BtBuA-1T, (b) BtBuA-2T. For the excitation wavelength of the photoluminescence the respective absorption maxima are used.

(a)

(b)
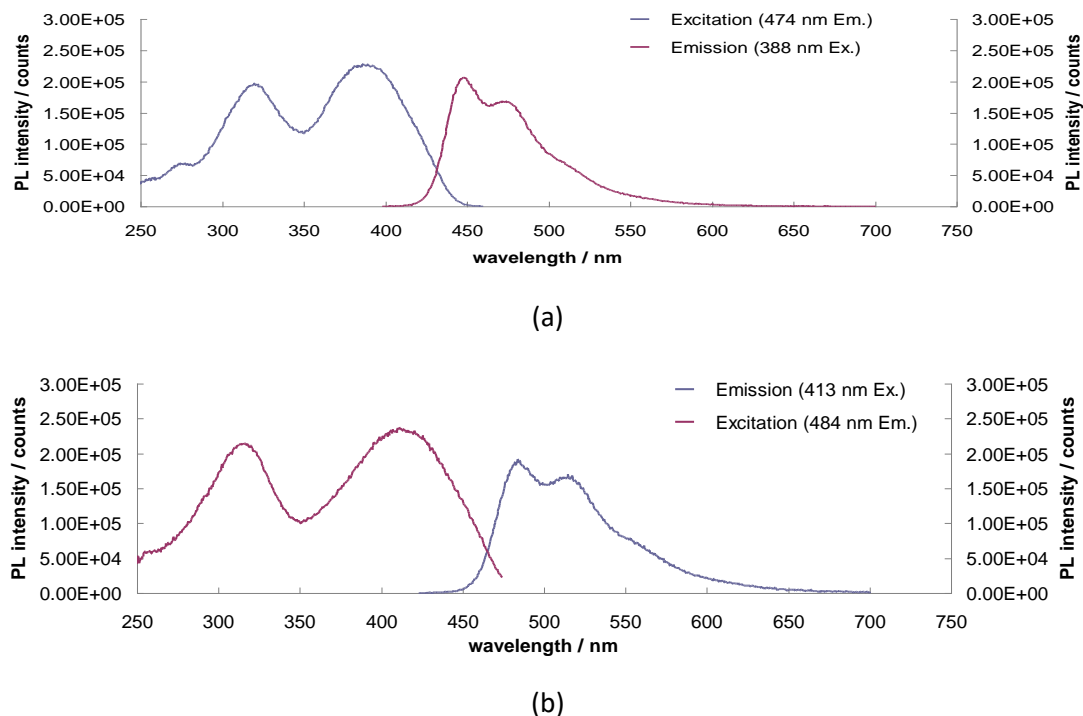
Figure 4.36: Absorption- and emission spectra of (a) BTMSA-1T, (b) BTMSA-2T. For the excitation wavelength of the photoluminescence the respective absorption maxima are used.
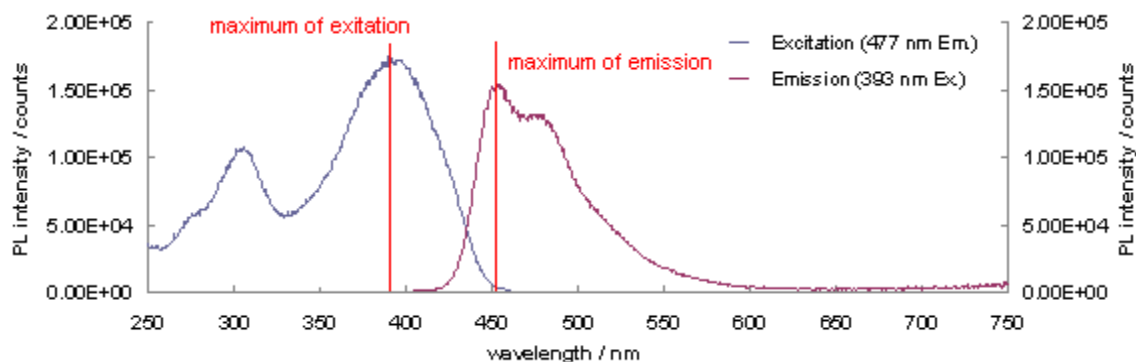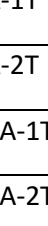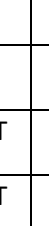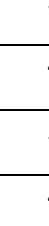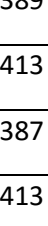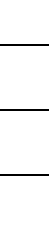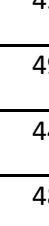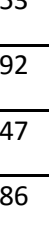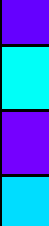
Figure 4.37: Methodology to evaluate the maximum of excitation and emission.

The graphs above are evaluated as shown in Figure 4.37. The maximum of excitation can be determined by measuring the wavelength of the peak with the highest wavelength of the excitation graph. On the other hand the maximum of emission can be determined by evaluating the wavelength of the peak with the lowest wavelength of the emission graph.

The maximum of excitation and emission are summarized in Table 4-7. The excitation wavelengths are in a range between 381nm and 437nm. The emission wavelengths of the materials have higher values ranging from 441nm to 514nm because of the Stoke's shift between absorption and emission. As it can be seen longer-chained molecules have the maximums of excitation and emission at higher wavelengths. This red shift of the longer-chained molecules depends on the amount of thiophene units and therefore on the size of the delocalized π-electron system.[33]

Substance	Maximum of excitation	1st maximum of emission	Color of 1st maximum	Calculated band-gap	2nd maximum of emission	Color of 2nd maximum
	nm	nm		eV	nm	
BMA-1T	392	453		2.74	480	
BMA-2T	419	488		2.54	516	
BMA-3T	437	514		2.41	545	
BHA-1T	385	441		2.81	468	
BHA-2T	414	481		2.58	510	
BHA-3T	433	507		2.45	542	
BFA-1T	381	442		2.81	465	
BFA-2T	407	478		2.60	507	
BMOA-1T	394	471		2.63	485	
BMOA-2T	420	499		2.49	522	
B^{t}BuA-1T	389	453		2.74	476	
B^{t}BuA-2T	413	492		2.52	519	
BTMSA-1T	387	447		2.78	475	
BTMSA-2T	413	486		2.55	516	

Table 4-7: Results of fluorescence measurements. maximums with longest wavelength and realted color.

The determination of the emission wavelength of a material gives information about the color of the excited substance. The measurement ensures that the investigated substances can be stimulated by higher energized photons. If the substance can also be electrically stimulated by applying a voltage the emission wavelength can only be determined with an electro-optical measurement.

4.2.3 Calculated energy levels

The combined characteristics of the energy levels which are necessary for the creation of an OLED are obtained by the HOMO level which was measured with the help of cyclic voltammetry, by the energy of the band gap which was measured with the help of photoluminescence measurement and by subtraction of HOMO level minus energy difference of the band gap which results in the LUMO level.

$$E_{LUMO} = E_{HOMO} + E_{BG} \tag{4-3}$$

	E_{LUMO}	Eg	E_{HOMO}	$\lambda_{Emission}$	color
	eV	eV	eV	nm	
BFA-1T	2,42	2,8	5,23	442	
BFA-2T	2,72	2,6	5,32	478	
BHA-1T	2,39	2,8	5,2	441	
BHA-2T	2,57	2,6	5,15	481	
BHA-3T	2,7	2,5	5,15	507	
BMA-1T	2,37	2,7	5,11	453	
BMA-2T	2,5	2,5	5,04	488	
BMA-3T	2,65	2,4	5,06	514	
BMOA-1T	2,23	2,6	4,86	471	
BMOA-2T	2,52	2,5	5,01	499	
BTBUA-1T	2,42	2,7	5,16	453	
BTBUA-2T	2,67	2,5	5,19	492	
BTMSA-1T	2,24	2,8	5,02	447	
BTMSA-2T	2,72	2,6	5,27	486	

Table 4-8: Summarization of the HOMO and LUMO energy levels as well as the wavelength and emission color of all organic materials.

The HOMO level ranges for all materials from 4,86 eV to 5,32 eV and the LUMO level from 2,23 eV to 2,72 eV. The color spectrum ranges from green to blue whereas longer chained molecules feature a smaller band gap and therefore a smaller wavelength. This results in a more greenish color of longer chained molecules. Nonetheless, because of the second maximum of the emission spectrum which can be seen in the previous chapter of the photoluminescence measurement the resulting output color of an OLED can appear more green.

4.2.4 Electrical and optical Characteristics

The electro-optical properties of the investigated substances are very important for the classification of the substances. If the materials can be electrically stimulated and emit light they are suitable for Light emitting devices such as LEDs and Screens. The material was contacted by an ITO anode and a magnesium cathode by building a simple diode. On a specially prepared needle prober the simple diode was contacted to apply voltage.

The selected design of the shadow mask offers the possibility of multiple measurements of the material at multiple dots of different sizes. Because of defects and degradation of the organic and the cathode material some of the dots do not result in a useful measurement.

Some areas of the slide show defects which result from not thoroughly solved basis materials as well as impurities as shown in Figure 4.38. As explained before this defects lead to a non-uniformity of the organic layer and result in a punch trough during the electric measurements.

a)   b)
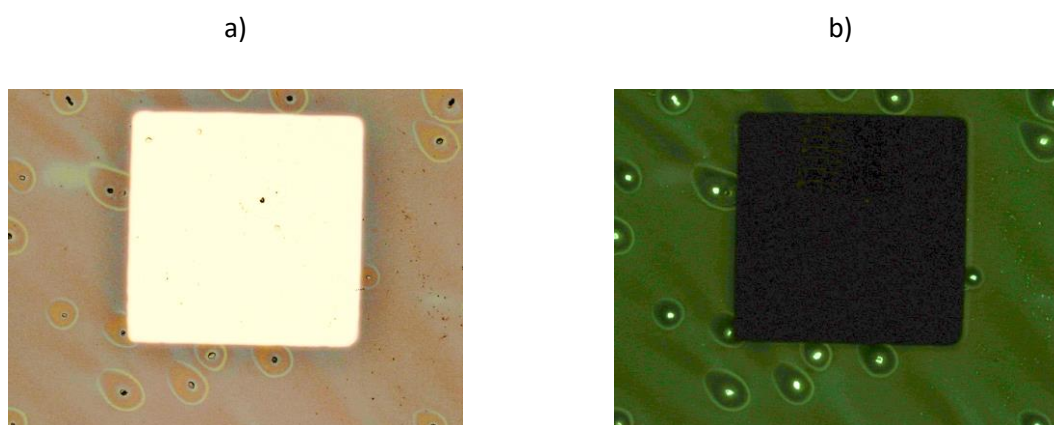
Figure 4.38: Defects of the organic material of an OLED examined with the microscope (a) under normal light and (b) stimulated with UV light.

Even with a defect-free organic layer a breakdown of the organic layer appears where the organic material degraded and the top electrode blister. This possibility of a breakdown of the organic material increases if constructed OLED is not tested immediately after fabrication. The alteration of the surface of the magnesium top electrode can be seen in Figure 4.39.

a)   b)

Figure 4.39: Microscope image of a top electrode (a) during normal operation and (b) after a breakdown of the organic material.

The graphs below are only measured at the dots with the size of 1x1mm² to be able to compare the results between the different materials. The photocurrent is measured by putting the sensor directly below the stimulated dot.
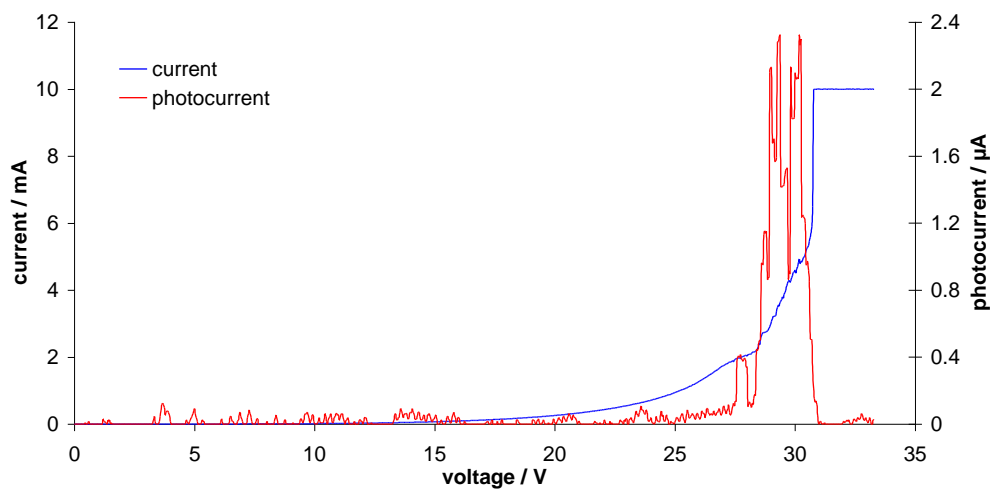
Figure 4.40: Measured graph of the current and photocurrent of BMA-1T.

Figure 4.41: Measured graph of the current and photocurrent of BMA-2T.

Figure 4.42: Measured graph of the current and photocurrent of BMA-3T.

The graphs of Figure 4.40, Figure 4.41 and Figure 4.42 show the voltage dependence of the BMA-nT substances. It can be seen that at longer chained molecules the current and photocurrent starts at a lower voltage. For BMA-1T 1mA current is attained at about 24V, for BMA-2T the voltage is about 17V and for BMA-3T it is about 8V. The light output of the substances shows nearly similar characteristics like the measured current. Impurities and contacting problems result in spikes which can be seen at the low voltages of BMA-2T as well as the high voltages of BMA-1T. The measured light output was very low. The photocurrent was within the 1μA range.

Figure 4.43: Measured graph of the current and photocurrent of BHA-2T.

Figure 4.44: Measured graph of the current and photocurrent of BHA-3T.

Figure 4.43 and Figure 4.44 show the characteristic of the BHA-nT materials. Unfortunately, it was not possible to measure the BHA-1T substance because of too less material available. In the graphs it can be seen that the measured current also rises at a lower voltage for the longer chained material. At higher voltages the materials mostly have a breakdown which results in a disappearance of the photocurrent. The high photocurrent peaks of BHA-3T result out of contacting problems which cause small breakdowns at the junction.
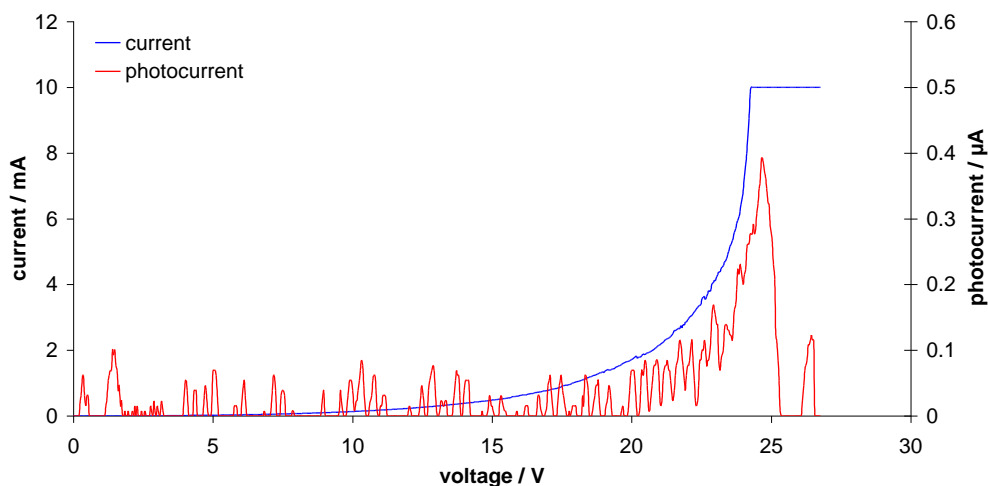
Figure 4.45: Measured graph of the current and photocurrent of BFA-2T.
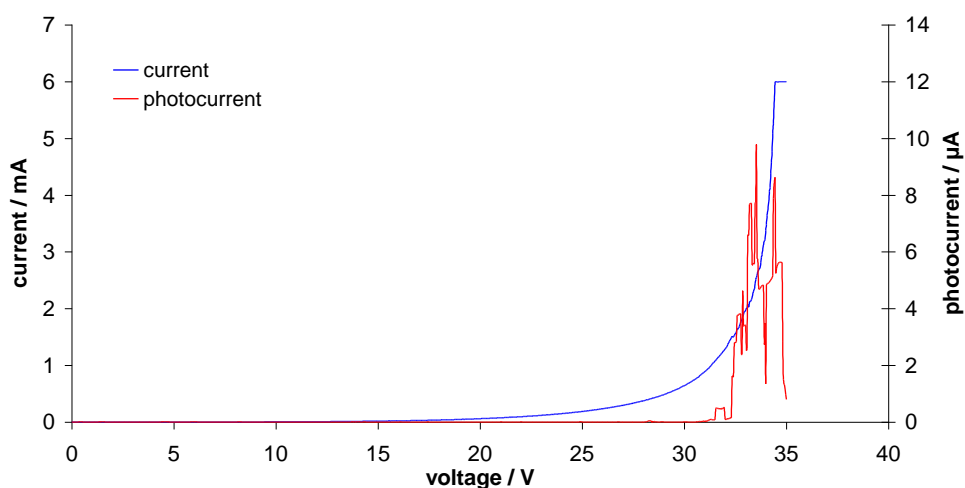
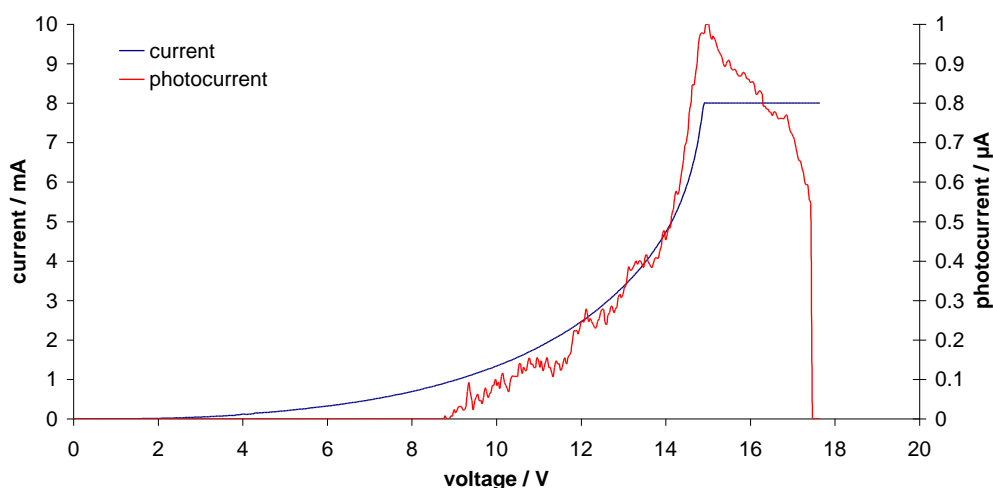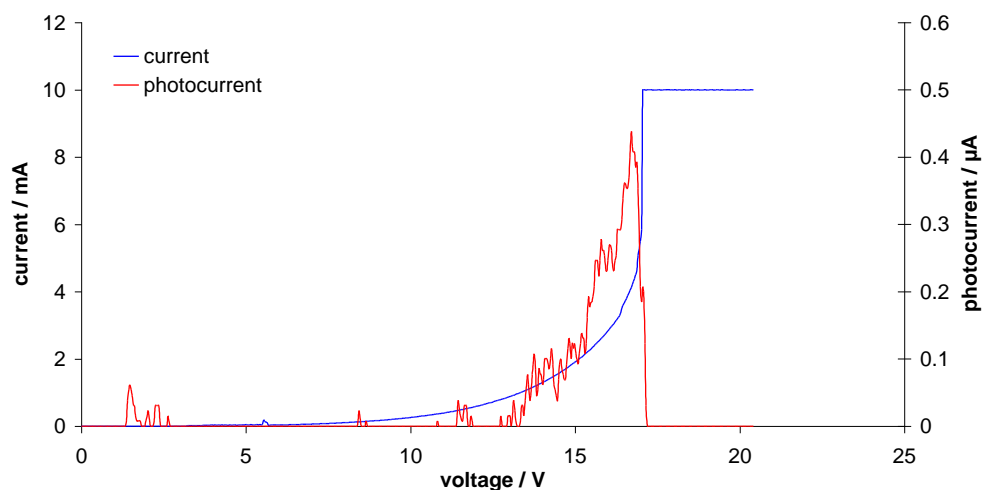**Figure 4.46: Measured graph of the current and photocurrent of BtBuA-1T.**

Figure 4.44 and Figure 4.45 show the graphs of BFA-2T and BtBuA-1T. The measurement of BFA-1T and BtBuA-2T can not be shown because of too less amount of the substance to get a homogeneous layer for an OLED. Both substances show response at very high voltages with very little light output.

Figure 4.47: Measured graph of the current and photocurrent of BTMSA-1T.

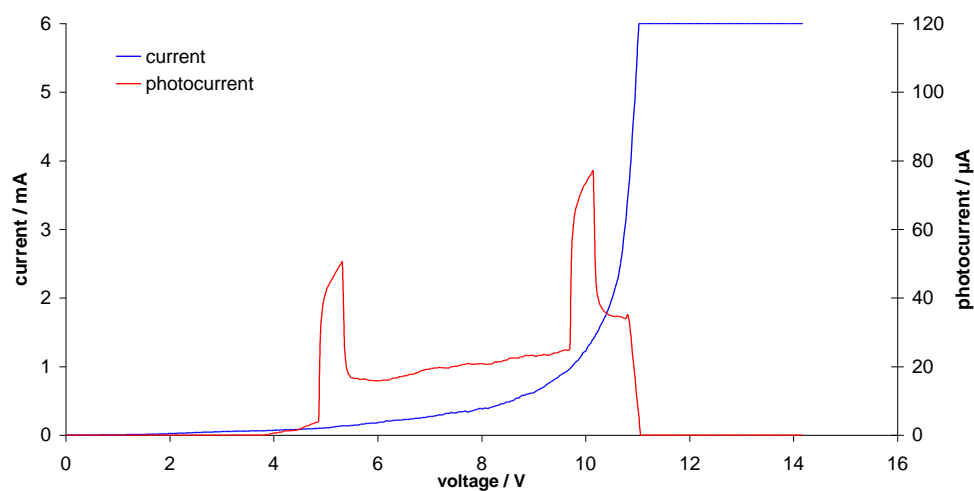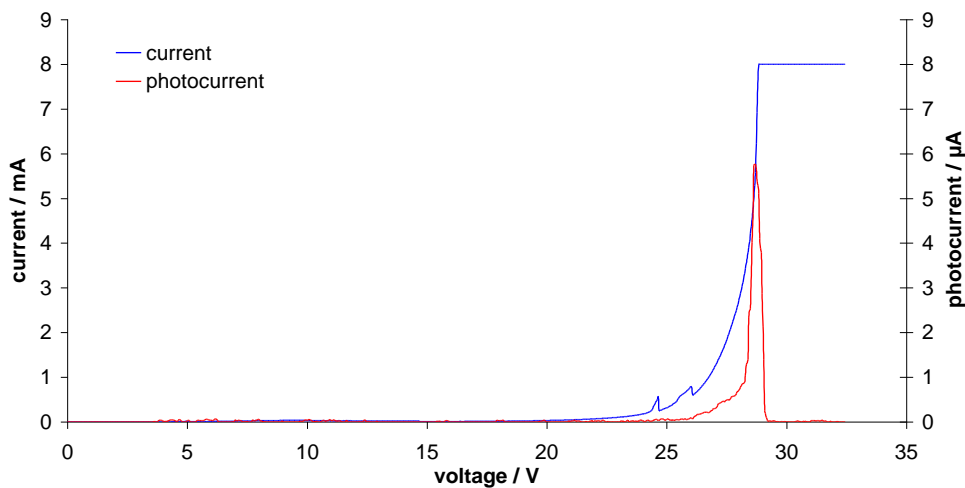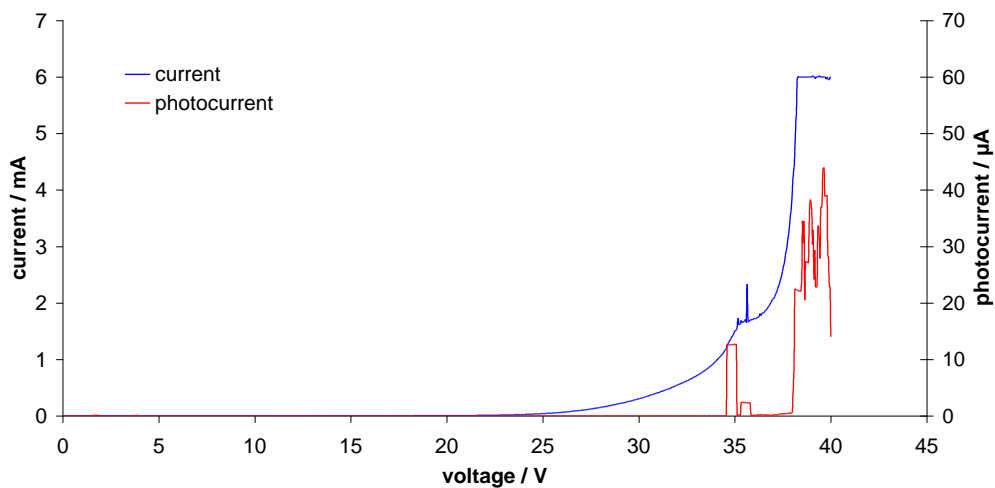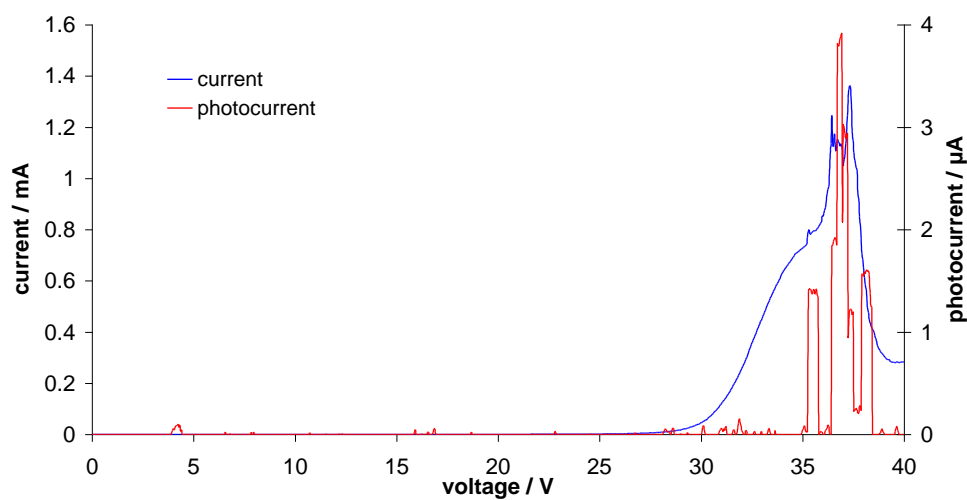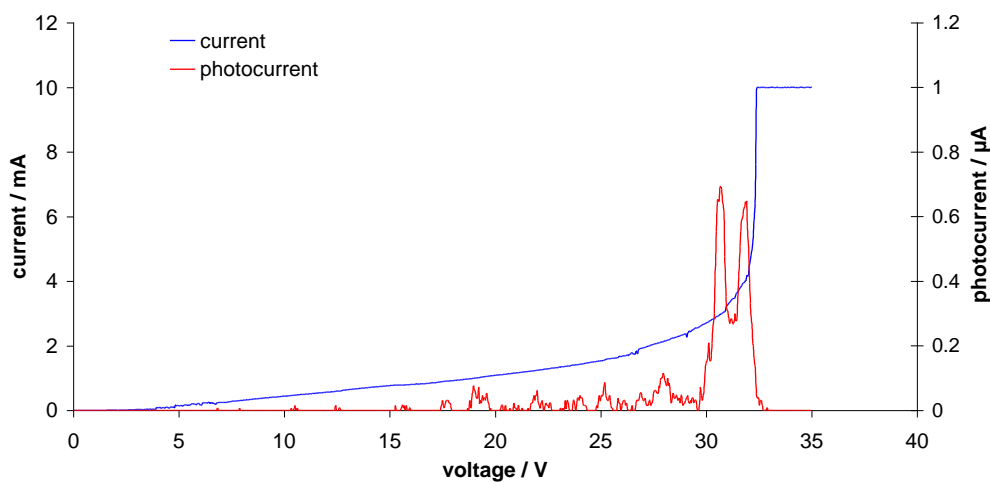**Figure 4.48: Measured graph of the current and photocurrent of BTMSA-2T.**

Figure 4.49: Measured graph of the current and photocurrent of BMOA-2T.
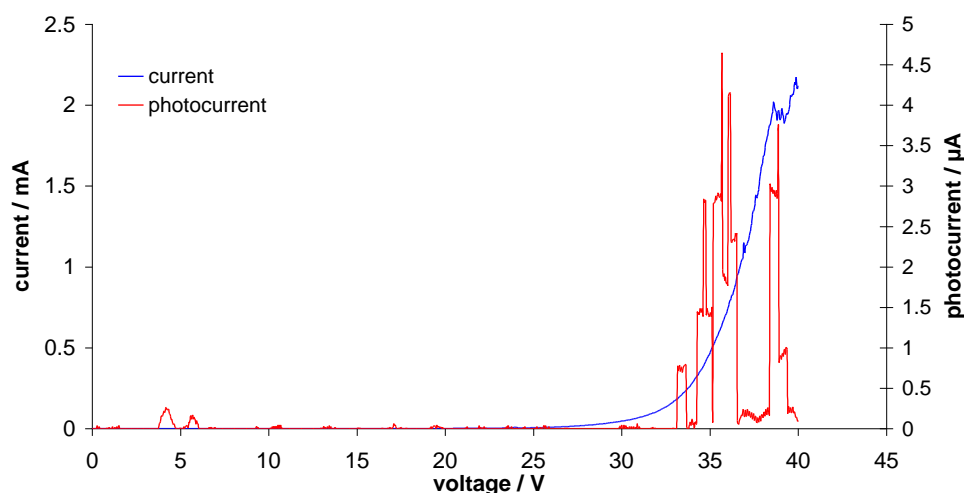
Figure 4.50: Measured graph of the current and photocurrent of CAH-1T .

For the materials BTMSA-nT the graphs of Figure 4.47 and Figure 4.48 show that the chain length does not have that much influence of the current to voltage graph as for BMA-nT. Moreover, both materials are very difficult to measure and show a lot of spikes which are mostly caused by contacting problems between the interfaces of needle and cathode as well as cathode an organic material. Therefore, the huge difference of the photocurrent can not only be traced back to the kind of the substance respectively the chain length.

The graph of BMOA-2T (Figure 4.49) shows a constant ascending slope of the current which can be explained by a resistive portion of the material but also by insufficient junction properties between the cathode and the material. A measureable photocurrent is only emitted at high voltages but is relatively low with the maximum below 1µA.

In Figure 4.50 the graph of CAH-1T show that the material works only at high voltages of over 30V. At the measurement the maximum voltage was restricted to 40V because otherwise a punch through of the organic layer is very probably. The current through the material does not exceed 2,5mA and the photocurrent does not show a very promising characteristic with many spikes and irregular behavior.

Generally the current and photocurrent measurements of the investigated substances show interesting behavior which can be suitable for some applications. For specific use of the substances in a device further measurements have to be done at different parameters such as the thickness of the organic layer, the working environment, the electrode material and so on. Especially the alteration and improvement of the cathode material as well as multilayer diodes should result in an improvement of the electrical characteristics in general and of the light output in particular.

5 Conclusion

The goal of this thesis is to develop and to optimize a process for spin coating an organic layer onto a transparent conductible substrate and to build up a demonstrator of the basic organic light emitting diode (OLED). For this purpose the used organic substances are characterized electro-chemically and optically to adjust the process parameters and to fabricate a device with a quantum output high enough to emit light. These results are used to proof the concept of a fabrication of an OLED by the use of the inexpensive and fast technique of spin-coating the organic layer.

The experiments for the fabrication and structuring of the different layers of the OLED device are performed under clean room conditions to prevent contamination of the biological layers. The process parameters for the spin-coating of the organic layer as well as the deposition of the top cathode material are experimentally developed respectively adopted from previous publications. The OLED demonstrator is fabricated on a glass substrate covered with a transparent conductive metal layer of indium tin oxide (ITO) which works as anode. Subsequently, the organic layer is spin-coated onto the glass slide and with the help of a shadow mask a structured metal cathode is deposited as top layer.

Previous to the fabrication of the device the energetic orbits of the organic substances are characterized to determine the metals which best fit as electrode materials. Therefore, the organic substances are analyzed by cyclic voltammetry to gain the HOMO energy level. Additionally, the characteristic wavelength and therefore the energy of the band gap between the HOMO and LUMO level is measured by UV-Vis spectroscopy as well as by photoluminescence spectroscopy. The resulting color spectrum of the organic molecules range from 512nm to 602nm whereas shorter chained molecules emit light at smaller wavelengths.

For the deposition of the organic layer the powdery substances are solved in the solvents Toluol and Chloroform at a well-defined concentration. To achieve good results the spin-coating process parameters such as the concentration of the substance, the type of solvent, the spin speed and the duration of the spin-coating are adjusted to obtain a homogeneous layer of a well-defined thickness. The thickness of the organic layer is crucial for the operation of the diode. If the organic layer is too thin the charge carriers recombine at the opposite electrodes and if the organic layer is too thick the quantum efficiency will decrease.

All deposited organic layers are characterized for their surface roughness and thickness to determine the ability to fabricate a diode without many defects. Unfortunately, measuring the thickness of the organic layer contactless by ellipsometry is not possible because of the nearly similar optical properties

of the organic layer, the transparent anode and the glass substrate. Thus, the thickness is determined with an AFM by scratching a hole into the organic layer and by measuring the height difference.

For the deposition of the top cathode material a shadow mask as well as a bracket is designed to structure the cathode material contactless during the deposition. Moreover, because of the use of a low work function material for the cathode such as magnesium a new evaporation device is constructed to reduce the risk of fast oxidation when interfering with air after the deposition process.

After the deposition of the top contact the diode is immediately characterized electrically and electro-optically to reduce the influence of the degradation of the organic layer and the magnesium at ambient air. The electro-optical measurements are done at a needle prober station with a specifically modified tip to prevent the puncturing of the thin cathode material. When performing the current-voltage ramping the materials show an exponential raising graph quite similar to non-organic photodiodes. The measured optical output of the organic diodes is quite low, a fact which can be referred generally to the basic design of the test arrangement and specifically to the single layer design of the OLED which offers only a very low efficiency.

Finally, the results of this work shows the feasibility to build OLEDs by spin-coating of the organic layer. Besides that, novel organic substances are characterized which show promising features for further use as organic semiconductors.

However, many interesting topics for the fabrication of an OLED remain open for future research like the fabrication of higher efficient multilayer devices, the passivation of the surface for a longer lifetime of the OLED, a more sophisticated bonding of the electrodes as well as the use of a flexible substrate.

Moreover, the integration of the constructed OLED into a complete Lab on a Chip (LoC) application could not be performed during this work but is part of the overall project of the research group which this work was part of. Anyhow, the successful fabrication of a fully functional OLED is a promising step toward a fully integrated LoC application to analyze bio-signals. Moreover, the realized structuring of the electrodes enables the fabrication of diode arrays for the accurate excitation of specific areas in a biosensor. Besides that, the low temperature fabrication processes which are used to assemble the OLED offers the possibility to easily transfer the optical stimulator to a flexible substrate.

Furthermore, the construction of a flexible electro-organic sensor which not only facilitates an organic stimulator to emit light but also an organic transistor to detect the incident light would be an interesting topic for future investigations.

6   References

[1]   Lochner C.M., Khan Y., Pierre A., Arias A.; "All-organic optoelectronic sensor for pulse oximetry", Nature Communications, December 2014

[2]   Steude A., Gather M.C.; "OLED microdisplays as biophotonics platform", Frontiers in Optics, 2014

[3]   M. Pope, H. P. Kallmann, P. Magnante; "Electroluminescence in Organic Crystals", J. Chem. Phys. 38, p. 2042, 1963

[4]   Tang, C.W., VanSlyke, S.A.; "Electroluminescence in Organic Crystals"; Appl. Phys. Lett. 51, p. 913, 1987

[5]   O. Prache, "Active matrix molecular OLED microdisplays"; Displays 22, p. 49-56, 2001

[6]   A. H. Davis , K. Bussmann; „Organic luminescent devices and magnetoelectronics";J. Appl. Phys., Vol. 93, No. 10; May 2003

[7]   G. Gu, V. Bulovic´, P. E. Burrows, S. R. Forrest;„Transparent organic light emitting devices"; Appl. Phys. Lett. 68 (19), May 1996

[8]   M. A. Baldo, S. Lamansky, P. E. Burrows, M. E. Thompson, S. R. Forrest;„Very high-efficiency green organic light-emitting devices based on electrophosphorescence";Appl. Phys. Lett. 75 (1), July 1999

[9]   C. Adachi, T. Matsushima, H. Nakanotani, D. Yokoyama, M. Yahiro; "Organic light emitting devices from OLED to organic laser diode";SC4.S5.3

[10]   J.L. Segura, „The chemistry of electroluminescent organic materials",Acta Polym. 1998, 49, 319 – 344

[11]   J. C. Scott, G. G. Malliarasab, J. R. Salema, P. J. Brocka, L. Bozano and S. A. Carter; "Injection, transport and recombination in organic light-emitting diodes";SPIE Vol. 3476, July 1998

[12]   Christoph Unterlechner; Dissertation: „Elektronische Eigenschaften von diskotischen Flüssigkristallen und segmentierten Poly(arylenvinylenen)", p. 10; Marburg/Lahn 1999

[13]   M.G.Mason et al; "Interfacial chemistry of Alq3 and LiF with reactive metals"; J. Appl. Phys., Vol. 89, No. 5, 1. March 2001

[14]   L.S. Hung, C.W. Tang, M.G. Mason; "Enhanced electron injection in organic electroluminescence devices using an Al/LiF electrode"; Appl. Phys. Lett. 70, p. 152, 1997

[15]   X. Zhou, M. Pfeiffer, J.S. Huang, J. Blochwitz-Nimoth, D.S. Qin, A. Werner, J. Drechsel, B. Maennig, K. Leo; "Low-voltage inverted transparent vacuum deposited organic light-emitting diodes using electrical doping " ; Appl. Phys. Lett., 81, p. 922, 2002

16 C. Unterlechner; „Systeme für organische Leuchtdioden: Elektronische Eigenschaften von diskotischen Flüssigkristallen und segmentierten Poly(arylenvinylenen)"; Dissertation, Marburg/Lahn 1999

17 R.R. Gagné, C.A. Koval, G.C. Lisensky; "Ferrocene as an Internat Standard for Electrochemical Measurements"; Inorg. Chem., 19, p. 2854-2866, 1980

18 J. Pommerehne, H. Vestweber, W. Guss, R.-F.-Mahrt, H. Bässler, M. Porsch, J. Daub; „Efficient two layer LEDs on a polymer blend basis"; Adv. Mater., 7, 551, 1995

19 http://www.files.chem.vt.edu/chem-ed/spec/uv-vis/singlebeam.html

20 http://www.itst.ucsb.edu/~vinhnguyen/Time-Frequency_Spectroscopy.htm

21 Roman, G.T.; Kennedy, R.T.; "Fully integrated microfluidic separations systems for biochemical analysis", J. Chromatogr. A 2007, 1168, 170–188

22 Yi, C.; Li, C.W.; Ji, S.; Yang, M.; "Microfluidics technology for manipulation and analysis of biological cells", Anal. Chim. Acta 2006, 560, 1–23

23 Haeberle, S.; Zengerle, R.; "Microfluidic platforms for lab-on-a-chip applications", Lab Chip 2007, 7, 1094–1110

24 Williams G., Backhouse C., Aziz H.; "Integration of Organic Light Emitting Diodes and Organic Photodetectors for Lab-on-a-Chip Bio-Detection Systems", Electronics 2014, 3, 43-75

25 Cai, Y.; Shinar, R.; Zhou, Z.; Shinar, J.; "Multianalyte sensor array based on an organic light emitting diode platform", Sensor. Actuat. B 2008, 134, 727–735

26 Cai, Y.; Smith, A.; Shinar, J.; Shinar, R.; "Data analysis and aging in phosphorescent oxygen-based sensors", Sensor. Actuat. B 2010, 146, 14–22

27 Cai, Y.; Shinar, R.; Zhou, Z.; Shinar, J.; "Multianalyte sensor array based on an organic light emitting diode platform", Sensor. Actuat. B 2008, 134, 727–735

28 Shuai, Y.; Banerjee, A.; Klotzkin, D.; Papautsky, I.; "On-Chip Fluorescence Detection with Organic Thin Film Devices for Disposable Lab-on-a-Chip Sensors", IEEE Sensors 2008, Proceedings of the Seventh IEEE Sensors Conference 2008, Lecce, Italy, 26–29 October 2008; IEEE: Piscataway, NJ, USA, 2008; pp 122–125

29 H.L. Skriver, N.M. Rosengard; „Surface energy and work function of elemental metals"; Physical Review B, Vol 46, Number 11; 15. September 1992

30 N.D. Lang, W. Kohn; „Theory of Metal Surfaces: Work Function"; Physical Review B, Volume3, Number 4; 15. Feb. 1971

31 Hamann, Vielstich; „Elektrochemie", Chapter 5.2.1 „Die Dreieckspannungsmethode", 1998

32   Johann Mößler; Dissertation „Synthesis, Spectroscopic Characterization and Electron Transfer Properties of Covalently Linked Chlorin- and Bacteriochlorin-Quinones as Model Compounds for Photosynthesis"; FU Berlin, 1999

33   D. Lumpi; „Strategien zur Synthese von α,ω-Bis(4-aminophenyl)-substituierten Oligothiophenen sowie Thiophen-Ringfragmentierungsprodukten als potentielle Materialien für Organic Electronics"; page 78; Nov. 2009